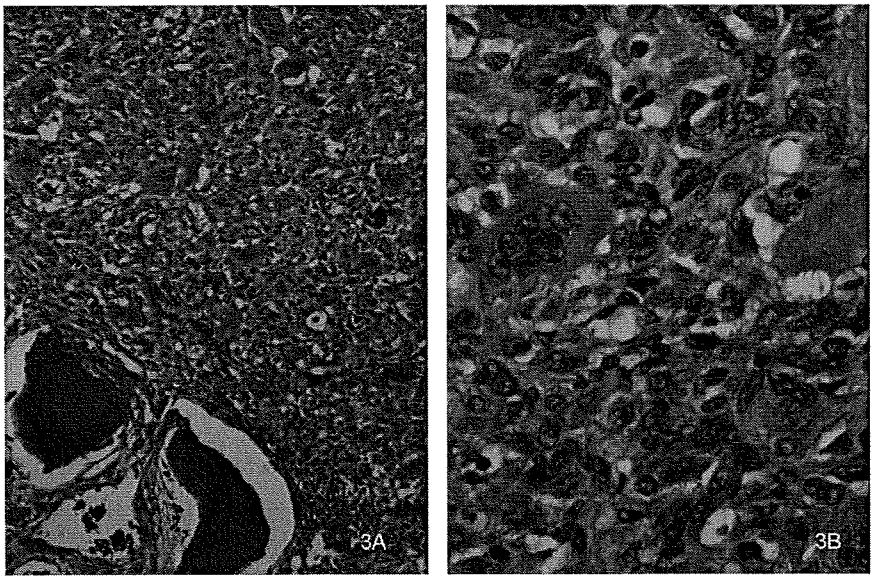

FIG. 3 (A) The recurrent tumour is composed of mononuclear stromal cells and multinucleated giant cells with foci of ectopic ossification (lower left) (H&E, ×100). (B) Higher magnification to demonstrate the mononuclear stromal cells with mild nuclear atypia. Scattered multinucleated giant cells are also present (H&E, ×400).

The patient is still alive 36 months after the second surgery, although the subsequent follow-up showed a 10 cm expansile sclerotic and osteolytic mass in the sacrum, mainly S1 and S2.

Kah-Wai Ngan
Wen-Yu Chuang
Chi-Ju Yeh

Department of Pathology, Chang Gung Memorial Hospital, Chang Gung University College of Medicine, Taoyuan, Taiwan

Contact Dr K-W. Ngan. E-mail: ngan751@hotmail.com

1. Leggon RE, Zlotecki R, Reith J, Scarboriugh MT. Giant cell tumor of the pelvis and sacrum. 17 cases and analysis of the literature. *Clin Orthop Relat Res* 2004; 423: 196–207.
2. Cooper KL, Beabout JW, Dahlin DC. Giant cell tumor: Ossification in soft tissue implants. *Radiology* 1984; 153: 597–602.
3. Lee FY, Montgomery M, Hazan EJ, Keel SB, Mankin HJ, Kattapuram S. Recurrent giant-cell tumor presenting as a soft-tissue mass. A report of four cases. *J Bone Joint Surg Am* 1999; 81: 703–7.
4. Ehara S, Nishida J, Abe M, Kawata Y, Saitoh H, Kattapuram SV. Ossified soft tissue recurrence of giant cell tumor of bone. *Clin Imaging* 1992; 16: 168–71.
5. Ross AE, Bojescul JA, Kuklo TR. Giant cell tumor: a case report of recurrence during pregnancy. *Spine* 2005; 30: 332–5.

DOI: 10.1080/00313020701813610

Giant chordoma occupying the whole abdominal cavity

Sir,

The natural history of chordoma is characterised by repeated episodes of local recurrence. Distant metastases may occur in the evolution of the disease. However, it is extremely unusual that the growth of chordoma occupies the abdominal cavity. We herein report an autopsy case of huge chordoma convoluting the whole peritoneal organs.

The patient was a 50-year-old male admitted to our hospital because of sacralgia and dysuria 10 years prior to death. The diagnosis of chordoma was confirmed by histological examination of the biopsy specimen, and subsequently sacral amputation was performed. He underwent enucleation of metastatic tumour of the liver 3 years prior to death, and local recurrence in the iliosacral region was removed 2 years prior to death. He had received no radiotherapy or chemotherapy. He presented with anorexia 2 months prior to death. Radiological examination showed that a huge mass filled the abdominal cavity. He died of the massive growth of the tumour.

At the post-mortem examination, his abdomen was markedly distended by the giant solid mass. The cut surface showed a lobular appearance with foci of haemorrhage, but no apparent necrosis (Fig. 1). We observed multiple metastatic lesions in the liver and both lungs, measuring up to hen's egg size. Microscopically, the tumour was composed of sheets of typical physaliphorous cells (Fig. 2A,B). No mitotic figures or necrosis were found (Fig. 2B). We could not detect dedifferentiated component in any of the lesions including the liver and lung metastases. Immunohistochemical staining of the tumour cells was positive for cytokeratin (AE1/AE3), vimentin, epithelial membrane antigen and S-100 protein. The MIB-1 index was less than 1%.

It has been reported that chordomas with an aggressive clinical course showed dedifferentiation to malignant fibrous histiocytoma, fibrosarcoma or osteosarcoma.[1–3] Although our case was clinically aggressive, the lesions were composed exclusively of conventional chordoma. In addition, adverse prognostic factors such as high MIB-1 index (>5%), necrosis, mitosis[4] and loss of lobular growth pattern[5] were not observed in this case. It remains unclear

why the histopathological findings didn't reflect the aggressive clinical course.

Junji Takeyama*
Hironobu Sasano†
Manabu Fukumoto‡

*Departments of Pathology, *Miyagi Children's Hospital, Aoba-ku, Sendai, †Tohoku University Hospital, Aoba-ku, Sendai, and ‡Institute of Development, Aging and Cancer, Tohoku University, Sendai, Japan*

Contact Dr J. Takeyama.
E-mail: jtakeyama@miyagi-children.or.jp

1. Fukuda T, Aihara T, Ban S, *et al.* Sacrococcygeal chordoma with a malignant spindle cell component. A report of two autopsy cases with a review of the literature. *Acta Pathol Jpn* 1992; 42: 448–53.
2. Hruban RH, May M, Marcove RC, *et al.* Lumbo-sacral chordoma with high-grade malignant cartilaginous and spindle cell components. *Am J Surg Pathol* 1990; 14: 384–9.
3. Meis JM, Raymond AK, Evans HL, *et al.* "Dedifferentiated" chordoma. A clinicopathologic and immunohistochemical study of three cases. *Am J Surg Pathol* 1987; 11: 516–25.

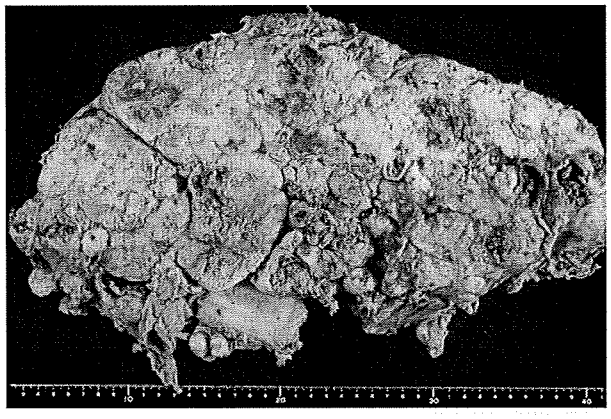

FIG. 1 The cut surface of the intra-abdominal mass, showing conglomerated tumour composed of lobules of various sizes.

4. Bergh P, Kindblom LG, Gunterberg B, *et al.* Prognostic factors in chordoma of the sacrum and mobile spine: a study of 39 patients. *Cancer* 2000; 88: 2122–34.
5. Naka T, Boltze C, Kuester D, *et al.* Intralesional fibrous septum in chordoma: a clinicopathologic and immunohistochemical study of 122 lesions. *Am J Clin Pathol* 2005; 124: 288–94.

DOI: 10.1080/00313020701813644

Merkel cell carcinoma with fibrosarcomatous differentiation

Sir,

Merkel cell carcinoma (MCC) is an aggressive cutaneous tumour that has a predilection for the sun-exposed skin of elderly patients.[1,2] Also called neuroendocrine carcinoma of the skin, it was initially thought to be a tumour of Merkel cells, the neuroendocrine cells of the skin, based on the ultrastructural finding of dense core granules within the tumour cells.[3] However, more recent evidence suggests an origin from pluripotential epidermal stem cells.[4,5]

Histologically, MCC is characterised by highly proliferative, small to intermediate-sized tumour cells with hyperchromatic nuclei, granular chromatin and scant cytoplasm that display both an epithelial and neuroendocrine immunochemical profile. Occasional cases of MCC have been reported to show focal areas exhibiting squamous, eccrine and melanocytic differentiation.[1,6,7] Sarcomatous differentiation in MCC is very rare and has only been reported in two cases previously: one case with leiomyosarcomatous differentiation[8] and another with a rhabdomyosarcomatous component.[9] A further unusual case of an atypical fibroxanthoma associated with a MCC has also been described which the authors considered most likely to represent a collision tumour (rather than divergent differentiation within a MCC).[10] MCC with undifferentiated spindle cell or fibrosarcomatous differentiation has not, to the best of our knowledge, been previously reported. We report one such case, make pathological comparisons with MCCs showing other lines of differentiation and briefly discuss the differential diagnosis of other malignant biphasic tumours of the skin.

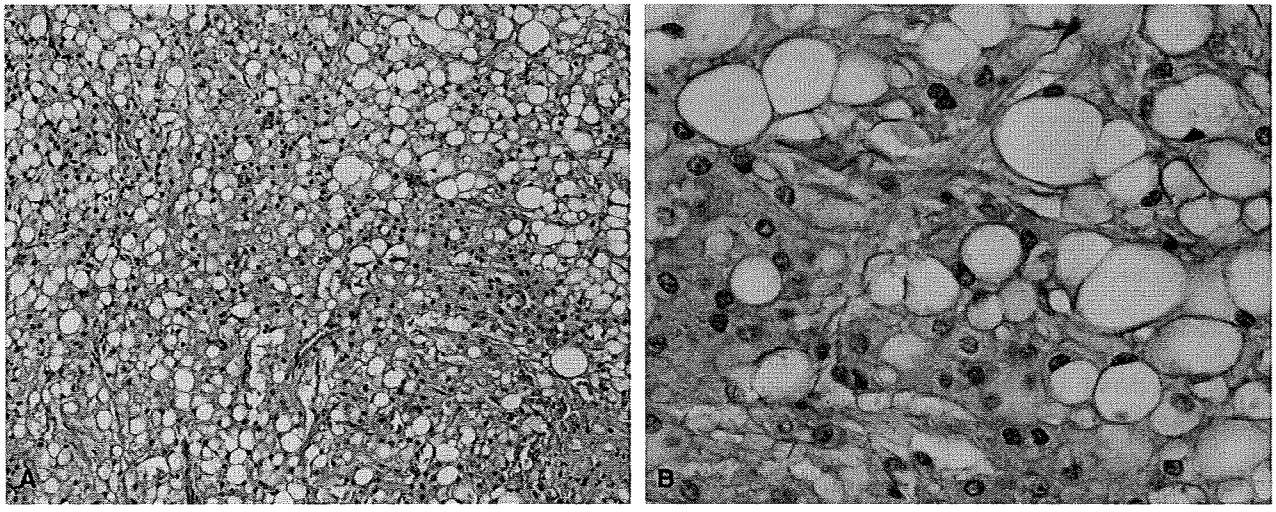

FIG. 2 (A) Low and (B) high power photomicrographs of a typical field from the lesion, showing physaliphorous cells with extracellular mucin (H&E).

The American Journal of Pathology, Vol. 173, No. 6, December 2008

DOI: 10.2353/ajpath.2008.080684

Neurobiology

Loss of Hrs in the Central Nervous System Causes Accumulation of Ubiquitinated Proteins and Neurodegeneration

Keiichi Tamai,[*†] Masafumi Toyoshima,[‡] Nobuyuki Tanaka,[*§††] Noriko Yamamoto,[‖] Yuji Owada,[‖] Hiroshi Kiyonari,[**] Kazuko Murata,[*] Yoshiyuki Ueno,[†] Masao Ono,[¶] Tooru Shimosegawa,[†] Nobuo Yaegashi,[‡] Masahiko Watanabe,[‡‡] and Kazuo Sugamura[*]

From the Departments of Microbiology and Immunology,[*] Gastroenterology,[†] Obstetrics and Gynecology,[‡] Cancer Science,[§] and Pathology,[¶] Tohoku University Graduate School of Medicine, Sendai; the Department of Organ Anatomy,[‖] Yamaguchi University Graduate School of Medicine, Yamaguchi; the Laboratory for Animal Resources and Genetic Engineering,[**] Center for Developmental Biology, Riken Kobe, Kobe; the Division of Immunology,[††] Miyagi Cancer Center Research Institute, Natori; and the Department of Anatomy,[‡‡] Hokkaido University School of Medicine, Sapporo, Japan

The endosomal sorting complex required for transport (ESCRT) proteins form multimolecular complexes that control multivesicular body formation, endosomal sorting, and transport ubiquitinated membrane proteins (including cell-surface receptors) to the endosomes for degradation. There is accumulating evidence that endosomal dysfunction is linked to neural cell degeneration *in vitro*, but little is known about the relationship between neural disorders and ESCRT proteins *in vivo*. Here we specifically deleted the *hrs* gene, ESCRT-0, in the neurons of mice by crossing *loxP*-flanked *hrs* mice with transgenic mice expressing the synapsin-I Cre protein (*SynI-cre*). Histological analyses revealed that both apoptosis and a loss of hippocampal CA3 pyramidal neurons occurred in the $hrs^{flox/flox}$;*SynI-cre* mice. Notably, the $hrs^{flox/flox}$;*SynI-cre* mice accumulated ubiquitinated proteins, such as glutamate receptors and an autophagy-regulating protein, p62. These molecules are particularly prominent in the hippocampal CA3 neurons and cerebral cortex with advancing age. Accordingly, we found that both locomotor activity and learning ability were severely reduced in the $hrs^{flox/flox}$;*SynI-cre* mice. These data suggest that Hrs plays an important role in neural cell survival *in vivo* and provide an animal model for neurodegenerative diseases that are known to be commonly affected by the generation of proteinaceous aggregates. *(Am J Pathol 2008, 173:1806–1817; DOI: 10.2353/ajpath.2008.080684)*

The generation of proteinaceous aggregates is a common pathological feature in neurodegenerative diseases.[1] Alterations in the lysosomal pathway are associated with normal brain aging, as well as with age-related neurodegenerative diseases, including Alzheimer's and Parkinson's. When the level of misfolded protein overwhelms the degradative pathways, cellular toxicity and neurodegeneration result.[2] Cellular mechanisms for degrading misfolded protein include the ubiquitin-proteasome system, which is the main nonlysosomal degradative pathway for ubiquitinated proteins, and autophagy, a lysosome-mediated degradative pathway.[3]

Glutamate receptors play prominent roles in several neurodegenerative diseases.[4–7] All *N*-methyl-D-aspartate (NMDA) receptors (NR) share one NR1 subunit and one or more NR2A-D and/or NR3 subunits, forming a heterotetrameric complex.[8] Fbx2-mediated ubiquitination is required for NR1 subunit degradation.[9] KEL-8, a substrate receptor for Cullin 3 ubiquitin ligases, is reported to be required for the proteolysis of the α-amino-3-hydroxy-5-methyl-isoxazolepropionic acid receptor (AMPAR) subunit GluR1.[10] Thus, ubiquitination is important for the homeostatic control of glutamate receptors in neurons.

Supported in part by the Ministry of Education, Culture, Sports, Science, and Technology of Japan (grants-in-aid for Scientific Research on Priority Areas 19041067 and 20012053 to N.T. and 19059001 to K.S.); the Japan Society for the Promotion of Science [grants-in-aid for Scientific Research (C) 19590484 to N.T. and 19590488 to K.M. and a grant-in-aid for Exploratory Research 19659108 to K.S.]; and the Naito Research Foundation.

Accepted for publication September 4, 2008.

Address reprint requests to Nobuyuki Tanaka, Department of Microbiology and Immunology, Tohoku University Graduate School of Medicine, 2-1 Seiryo-machi, Aoba-ku, Sendai, 980-8575 Japan. E-mail: n-tanaka@m.tains.tohoku.ac.jp.

Endosomal sorting complex required for transport (ESCRT) proteins form multimolecular complexes that control multivesicular body formation and transport ubiquitinated membrane proteins to the endosomes. The ESCRTs are subdivided into four complexes.[11] Ubiquitinated cargos such as epidermal growth factor receptors are initially recognized by the ESCRT-0 complex, and then sequentially handed off to ESCRT-I, -II, and -III. After these steps, the cargos are invaginated into multivesicular bodies and eventually sorted into the lysosomes. The ESCRT-0 component Hrs (also known as Hgs) plays a particularly major role in this sorting process.[12] Although several studies using Hrs mutants or its deletion in mammalian cells and mice suggest that it has a role in morphogenesis and development,[13,14] whether or not Hrs possesses any function in the nervous system is unknown.

Recent studies suggest that protein ubiquitination is essential for proper nervous system function.[15] Ubiquitination is a key tagging process for proper protein trafficking and turnover involving proteasome- and lysosome-dependent degradation. In addition, a recent study suggested that normal multivesicular body function is essential for neural cells to avoid degeneration.[16] Furthermore, ESCRT-III dysfunction is associated with a type of neurodegeneration that resembles frontotemporal dementia and other age-dependent neurodegenerative diseases.[17] These findings together highlight ESCRT function as being important for maintaining neuronal homeostasis, and prompted us to investigate the *in vivo* role of Hrs in the central nervous system. Using the Cre-loxP system, we found that Hrs is required for the degradation of ubiquitinated proteins in the central nervous system and the survival of mouse hippocampal CA3 neurons.

Materials and Methods

Generation of Floxed Hrs Mice

To generate a neuron-specific conditional knockout of Hrs (accession no. CDB0476K; Center for Developmental Biology, Kobe, Japan), we generated a floxed *hrs* allele (hrs^{flox}) using embryonic stem (ES) cell homologous recombination technology. For the targeting construct of the $hrs^{flox/flox}$ line, a C57BL/6J genomic clone was used to generate the *hrs* targeting vector, and two *loxP* sites were integrated, one upstream of exon 2 and one downstream of exon 4. The targeting vector was electroporated into TT2 ES cells, followed by G418 selection. Colonies surviving selection were tested for homologous recombination and incorporation of the *loxP* sites by Southern blot hybridization. Two clones were identified and injected into ICR 8 cell-stage embryos.[18] Chimeric mice were mated to C57BL/6J mice to identify germ-line transmission of the targeted *hrs* allele. Removal of the neomycin selection cassette, which was surrounded by *FRT* (Flp recombinase target) sites, was accomplished by first mating $hrs^{flox/flox}$ mice to FLPeR mice[19] at Riken (Kobe, Japan). All animal experiments were performed according to the guidelines laid down by the animal welfare committees of the Tohoku University Graduate School of Medicine and Riken.

Generation of $hrs^{flox/flox}$;Synl-cre Mice

Synl-cre transgenic mice (a gift from Jamey Marth, University of California, San Diego, CA)[20] were mated with the $hrs^{flox/flox}$ mice to generate $hrs^{flox/+}$;*Synl-cre* mice. The $hrs^{flox/+}$;*Synl-cre* mice were then mated with each other. Offspring carrying $hrs^{flox/flox}$;*Synl-cre* and $hrs^{+/+}$;*Synl-cre* were used for further analyses. These mice were genotyped by polymerase chain reaction (PCR) using DNA obtained from the tail.

Southern Blot Analysis

Genomic DNA from ES cells was digested with restriction enzymes, separated by electrophoresis on a 0.6% agarose gel, transferred to Hybond-N (GE Health Care, Chalfont St. Giles, UK, and hybridized with the random-primed probe.

Genotype Analysis

Genomic DNA from the mouse tail was used for PCR analysis. We genotyped the *hrs* flox allele using a forward primer (5′-GATGATGAGATGTTTACC-3′) and a reverse primer (5′-TTGTCCTTTACCTCTTAG-3′) that flank the 5′ *loxP* site. The PCR products were 354 bp for the $hrs^{flox/flox}$ allele and 229 bp for the wild-type allele. We amplified the $hrs^{\Delta 2-4}$ allele using a forward (6851F: 5′-TTGTTGAATGAGTAACAAGGGTGGT-3′) and reverse primer (9100R: 5′-TGGATCCCATGAAATGGGGAACAGC-3′). The PCR products were 0.3 kbp for the $hrs^{\Delta 2-4}$ allele and 2.3 kbp for the wild-type allele. Genotyping for the presence of the *Synl-cre* allele was performed using the following primer pair: forward (5′-TTACCGGTCGATGCAACGAGTGAT-3′) and reverse (5′-TTCCATGAGTGAACGAACCTGGTC-3′).

Western Blotting

Immunoblotting was performed as previously described.[21] In brief, brains from mice were homogenized in lysis buffer [1% Nonidet P-40, 20 mmol/L Tris-HCl (pH 7.5), 150 mmol/L NaCl, 1 mmol/L ethylenediaminetetraacetic acid, 1 mmol/L Na_3VO_4, 1 mmol/L phenylmethyl sulfonyl fluoride, and 20 μg/ml aprotinin]. The lysates were precleared by centrifugation (10,000 $\times$ *g*) for 20 minutes at 4°C. The supernatants were then separated by sodium dodecyl sulfate-polyacrylamide gel electrophoresis and transferred onto polyvinylidene difluoride membranes (Millipore, Billerica, MA). After being blocked with 5% nonfat milk in Tris-buffered saline containing 0.1% Tween 20, the membranes were probed with the indicated primary antibodies. After another wash, the membranes were probed with horseradish peroxidase-conjugated secondary antibodies (Cell Signaling, Beverly, MA).

Histology and Immunohistochemistry

Mice were perfused with 4% paraformaldehyde, and the dissected brains were postfixed for 24 hours before being embedded in paraffin. For histological analyses, 3-μm sections were stained with hematoxylin and eosin (H&E). Immunostaining was performed by the streptavidin-biotin immunoperoxidase method (Histofine SAB-PO kit; Nichirei, Tokyo, Japan) using primary antibodies. We used the antibodies at the following dilutions: anti-ubiquitin [1:200, 1B3, mouse monoclonal antibody (mAb); MBL International, Woburn, MA]; anti-ubiquitin (1:200, FK2, mAb; Biomol, Plymouth Meeting, PA); anti-GFAP (1:200, mouse mAb; Chemicon, Temecula, CA); anti-calbindin (1:200, rabbit polyclonal antibody; Chemicon). We also used anti-Hrs,[22] anti-NR1,[23] anti-NR2B,[24] and anti-GluR1 antibodies[25] as previously described. To detect mouse monoclonal antibodies, the Histofine mouse staining kit (Nichirei) was used. Immunoreactions were visualized with 3,3,-diaminobenzidine. For terminal deoxynucleotidyltransferase-mediated dUTP-biotin nick-end labeling (TUNEL) assays, 5-μm sections were deparaffinized, and terminal transferase labeling of the fragmented DNA was performed with an *in situ* cell death detection kit (Fluorescein; Roche, Indianapolis, IN), according to the assay protocol of the kit.

Reverse Transcriptase (RT)-PCR

RT-PCR was performed as previously described.[26] In brief, the total RNA from the brains of 8-week-old *hrs*$^{+/+}$; *Synl-cre* and *hrs*$^{flox/flox}$;*Synl-cre* mice was prepared using TRIzol (Invitrogen, Carlsbad, CA). PCR was performed in a 50-μl mixture consisting of 20 mmol/L Tris-HCl (pH 8.0), 2 mmol/L $MgCl_2$,50 mmol/L KCl, 0.2 mmol/L deoxynucleotide triphosphate mixture, 1 μmol/L of various primers, 1.25 U of Ex-TaqDNA polymerase (Takara Shuzo, Kyoto, Japan), and 1 μl of the RT reaction mixture as a template. The PCR conditions were as follows: denaturation at 94°C for 2 minutes, followed by 35 cycles of 30 seconds at 94°C, 1 minute at 65°C, and 1 minute at 72°C. The following oligonucleotide primers were used: HrsE1F (5′-GAGGCAGCGGCACCTTCGAG-3′) and HrsE7R (5′-ATGGCATTCCTCAGCATCCA-3′).

In Situ *Hybridization*

In situ hybridization was performed as previously described.[27] Mice were anesthetized and perfused with 4% paraformaldehyde. The brains were postfixed overnight at 4°C and then cryoprotected with 30% sucrose in 0.1 M phosphate buffer at 4°C. Frozen sections were cut at 20 μm on a freezing microtome and mounted on MAS-coated slides (Matsunami, Osaka, Japan). The transcription reactions were performed using a digoxigenin (DIG) RNA labeling kit (SP6/T7) (Roche). The purified plasmids were linearized and then used as templates for *in vitro* transcription of the DIG-labeled antisense (or sense control) RNA probes with T7 (or SP6) RNA polymerase. The transcripts were subjected to alkaline hydrolysis to reduce their size. For this, the DIG-labeled full-length cRNA was added to alkaline hydrolysis solution [40 mmol/L $NaHCO_3$/60 mmol/L Na_2CO_3 (pH 10.2)] and incubated for 15 minutes at 60°C. For *in situ* hybridization, the sections were postfixed in 4% paraformaldehyde [freshly prepared in 0.1 mol/L phosphate buffer (pH 7.4)] for 10 minutes, washed three times with phosphate-buffered saline (PBS), treated with 0.5 μg/ml proteinase K (Sigma) for 30 minutes at 37°C, postfixed in 4% paraformaldehyde for 5 minutes, washed three times with PBS, acetylated for 10 minutes, treated 0.3% Triton X-100 for 20 minutes, and washed three times with PBS for 5 minutes each. Prehybridization was performed for 1 hour at 65°C with hybridization buffer without probe and then hybridization was done at 65°C overnight in a new hybridization buffer containing one of the DIG-labeled RNA probes. The hybridization buffer consisted of 5× saline sodium citrate (SSC; Gibco BRL/Invitrogen, Tokyo, Japan), 50% deionized formamide (Sigma, St. Louis, MO), 500 μg/ml herring sperm DNA (Roche), 5× Denhardt's solution (Open Biosystems, Huntsville, AL), and 250 μg/ml transfer RNA (Roche). After hybridization, the sections were sequentially treated with 2× SSC/50% formamide for 30 minutes at 65°C, 2× SSC for 30 minutes at 65°C twice, and 0.2× SSC for 5 minutes at room temperature. The hybridized probe was detected with an alkaline phosphatase-conjugated anti-DIG antibody using a DIG nucleic acid detection kit (Roche) according to the manufacturer's protocol.

Behavioral Tests

All behavioral experiments were performed with 2- to 3-month-old male mice with a mixed 129/Ola-C57BL/6 genetic background and in the light phase of their diurnal cycle, between 09:00 and 17:00 hours. All experimental protocols were approved by the Animal Care Committee of the Tohoku University School of Medicine, and all experiments were performed in compliance with the relevant laws and institutional guidelines.

Open Field Test

Mouse locomotor activity in the open field was measured using a photo-beam system (BTA-1, Muromachi-Kikai, Tokyo, Japan). The values for ambulation distance were accumulated for 30 minutes and logged onto a personal computer.

Step-Through Passive Avoidance Test

The learning ability of the mice was evaluated using a step-through passive avoidance memory test, as previously described.[28] The training apparatus was a box consisting of a small lighted compartment (15 × 10 × 10 cm^3) and a large dark compartment (18 × 12 × 10 cm^3). A 10 × 10 cm^2 guillotine door separated the two compartments. The light compartment was made of clear Plexiglas, and was illuminated by a lamp (60 W) from the outside. The dark compartment had a series of stainless-

steel rods (3 mm in diameter, 1 cm apart) through which a constant electrical current could be delivered. The mice were first habituated to the box on 2 consecutive days. On the first day, they were placed in the light compartment and allowed to explore the box. The latency period for entering the dark compartment was recorded. As soon as a mouse entered the dark compartment, the door was closed, and the mouse was kept inside for 15 seconds before being returned to its cage. On the second training day, on entry into the dark compartment, the mice were given 0.5 mA of current for 5 seconds. The test session was performed 24 hours after the training session using the same paradigm, but without the foot shock. The latency period for each mouse to move into the dark compartment was recorded for up to a maximum of 300 seconds.

Wire Hanging Test

The ability of mice to hang upside down from a wire screen was tested as previously described.[29] The wires were 1 mm in diameter and spaced 1 cm apart. A rectangular area of the screen was taped off to confine the mouse to an 18 × 26 cm section of the screen. After a mouse was placed on the screen, the screen was waved gently in the air three times to force the mouse to grip the wires. The screen was then immediately turned upside down, 70 cm above a large rodent housing cage. The latency period for the mouse to fall into the cage was recorded. Mice that did not fall during the 60-second trial period were removed and given a maximal score of 60 seconds.

Forced Swimming Test

Mice were individually forced to swim in an aquarium (25 × 40 × 20 cm) containing 15-cm-deep water at 25 ± 1°C; the total duration of mouse immobility was measured during a 6-minute test.[30] Each mouse was judged to be immobile when it ceased struggling and remained floating motionless in the water, making only those movements necessary to keep its head above water.

Footprint Analysis

Footprint assessment was performed to detect gait abnormalities that could contribute to deficits in motor coordination on land.[31] Each hindpaw was colored black and forepaw red using nontoxic dye. For each mouse, five or more consecutive strides were averaged.

Results

Expression of Hrs in Mouse Brain

We first performed *in situ* hybridization to examine the expression of the *hrs* gene in the central nervous system because currently there is no antibody to reliably detect Hrs in brain tissue. In 5-week-old wild-type mice, *hrs* was ubiquitously expressed in the brain, with higher expression in the hippocampus, cerebral cortex, and hypothalamus (Figure 1, A and F). The degree of expression was higher in the CA3 than in the CA1 subfield in the hippocampus (Figure 1, B and C). Distinct expression was seen in the Purkinje cells (Figure 1, D and E).

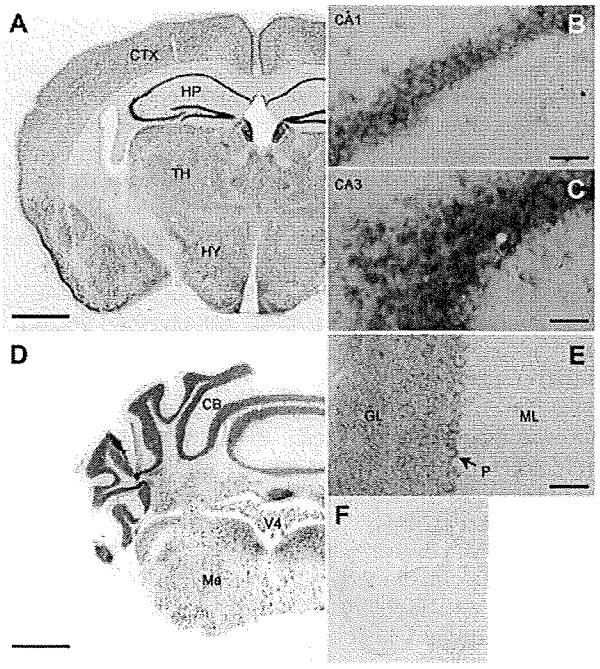

Figure 1. *In situ* hybridization of 5-week-old wild-type mouse brain probed for *hrs* mRNA. **A:** Coronal section through the cerebrum (hippocampus) showing the ubiquitous expression of *hrs* mRNA. Stronger *hrs* expression was seen in the CA3 (**C**) than the CA1 (**B**) subfield. **D** and **E:** Coronal section through the cerebellum showing strong expression of *hrs* in the granular cell layers and Purkinje cells. **F:** *In situ* hybridization of the section consecutive to **A** with the sense probe as a negative control. CTX, cerebral cortex; HP, hippocampus; TH, thalamus; HY, hypothalamus; CB, cerebellum; V4, fourth ventricle; Me, medulla oblongata; GL, granular layer; P, Purkinje cell; ML, molecular layer. Scale bars: 1 mm (**A**, **D**); 50 μm (**B**, **C**, **E**). Original magnifications: ×40 (**A**, **D**); ×400 (**B**, **C**, **E**).

Deletion of Hrs in the Central Nervous System

An *hrs* flox mouse was generated with *loxP* sites flanking exons 2 to 4 of the mouse *hrs* locus (Figure 2A). Heterozygous *hrs* flox ES cells were identified by Southern blot analysis (Figure 2B). To delete *hrs* specifically in the mouse brain, homozygous *hrs* flox mice ($hrs^{loxP/loxP}$) were crossed with *Synl-cre* transgenic mice. To assess whether exons 2 to 4 were deleted, we performed RT-PCR analysis of the brains from $hrs^{loxP/loxP}$;*Synl-cre*, and $hrs^{+/+}$;*Synl-cre* mice. A pair of primers spanning exons 1 and 7, respectively, amplified a 491-bp fragment from the $hrs^{+/+}$;*Synl-cre* brain and a 237-bp fragment from the $hrs^{loxP/loxP}$;*Synl-cre* brain (Figure 2C). Sequence analyses of the RT-PCR fragments showed that the *hrs* mRNA transcript from the $hrs^{loxP/loxP}$;*Synl-cre* brain contained a deletion of nucleotides 74 through 327, resulting in a frameshift and a stop codon in exon 5 (data not shown). PCR analyses of the genomic DNA from these brains revealed 0.3-kbp fragments (Figure 2D). Moreover, im-

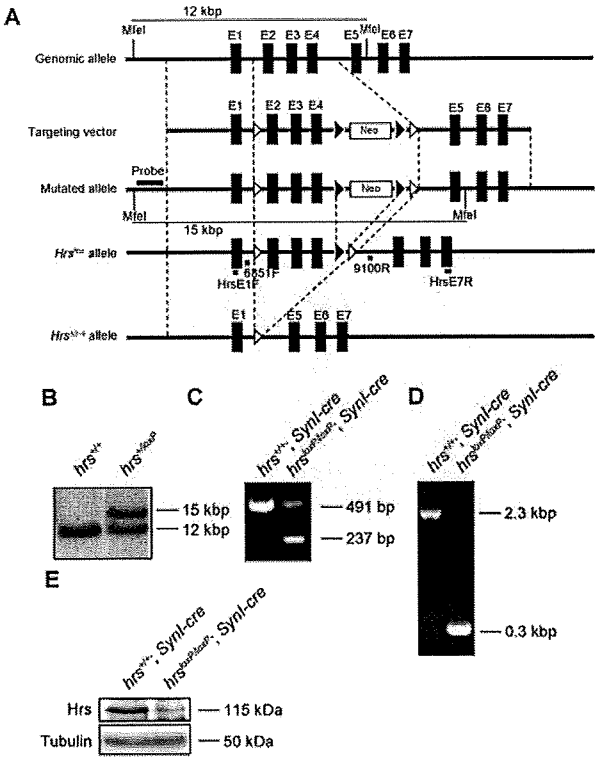

Figure 2. Generation of floxed *hrs* mice. **A:** Schematic representation of the *hrs* genomic locus, targeting vector, and *hrs* mutated locus. The targeting vector was designed to replace exon 2 (E2) to E4, which encode Hrs amino acids 74 to 327. The expected fragments generated by *MfeI* digestion were 12 and 15 kb for the wild-type and mutated alleles, respectively. **Open** and **closed arrowheads** denote the positions of the *loxP* and *FRT* sequences, respectively. **B:** Southern blot analysis of the *hrs* mutation in ES cell clones. DNA was digested with *MfeI*, and the blot was probed with the flanking 5′ probe as shown in **A**. Lines indicate the positions of the DNA fragments corresponding to the wild-type and mutated alleles. **C:** RT-PCR analysis of the total RNA from the brains of $hrs^{+/+}$;*Synl-cre* and $hrs^{loxP/loxP}$;*Synl-cre* mice. The primers used were HrsE1F and HrsE7R (see Materials and Methods). **D:** Genomic PCR analysis of the $hrs^{+/+}$;*Synl-cre* and $hrs^{loxP/loxP}$;*Synl-cre* brains. The primers used were 6851F and 9100R (see Materials and Methods). **E:** Western blot analysis for Hrs. Lysates from $hrs^{+/+}$;*Synl-cre* and $hrs^{loxP/loxP}$;*Synl-cre* brains were separated by sodium dodecyl sulfate-polyacrylamide gel electrophoresis and blotted with an anti-Hrs antibody.

munoblotting analysis with an anti-Hrs mAb revealed that ~60% of the Hrs expression was suppressed in the $hrs^{loxP/loxP}$;*Synl-cre* brain (Figure 2E). Because *Synl-cre* transgenic mice specifically express Cre recombinase in differentiated neurons, and not in astroglia,[20] these data suggest that both neurons and glial cells express Hrs. We conclude that the *hrs* flox allele represents a functional conditional allele.

Loss of Weight in Hrs Mutant Mice

$Hrs^{loxP/loxP}$;*Synl-cre* mice were morphologically indistinguishable from their littermates at birth. $Hrs^{+/+}$;*Synl-cre*, $hrs^{+/loxP}$;*Synl-cre*, and $hrs^{loxP/loxP}$;*Synl-cre* mice were obtained at the expected Mendelian ratios and were viable at least for several months. $Hrs^{+/loxP}$;*Synl-cre* mice did not differ in growth or behavior from their $hrs^{+/+}$;*Synl-cre* littermates. However, growth retardation of the $hrs^{loxP/loxP}$;*Synl-cre* mice became detectable by 3 weeks of age and gradually worsened; most of the $hrs^{loxP/loxP}$;*Synl-cre* mice did not show any increase in their body weight after they reached 8 weeks of age (Figure 3). Moreover, the $hrs^{loxP/loxP}$;*Synl-cre* mice were infertile.

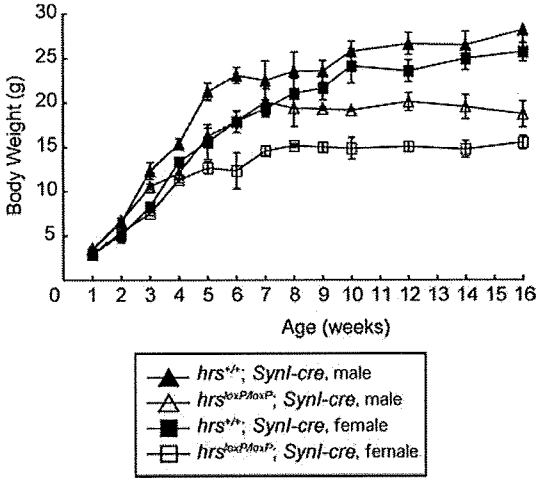

Figure 3. Phenotypes of the $hrs^{loxP/loxP}$;*Synl-cre* mice. Growth curves for $hrs^{+/+}$;*Synl-cre* (males, $n = 12$; females, $n = 9$) and $hrs^{loxP/loxP}$;*Synl-cre* (males, $n = 10$; females, $n = 9$) mice. Error bars indicate SE.

Loss of Pyramidal Neurons in the Hippocampal CA3 Subfield in Hrs Mutant Mice

We next performed histopathological examinations of the $hrs^{+/+}$;*Synl-cre* and $hrs^{loxP/loxP}$;*Synl-cre* mice by Nissl staining with cresyl violet. The gross anatomy of the Hrs mutant brain was normal. In the 2- and 3-week old brains, no histopathological difference was observed between the $hrs^{+/+}$;*Synl-cre* and $hrs^{loxP/loxP}$;*Synl-cre* mice (Figure 4, A–D). However, the number of pyramidal neurons in the hippocampal CA3 subfield was reduced in the 5-week-old $hrs^{loxP/loxP}$;*Synl-cre* brain (Figure 4, E and F), and progressive decreases were observed in the 8- and 28-week-old $hrs^{loxP/loxP}$;*Synl-cre* brains (Figure 4, G–J). In contrast, we could not detect any decrease in the pyramidal neurons in CA1. No difference was observed in any other regions, including the cerebral cortex, substantia nigra, striatum, cerebellum, or hypothalamus by Nissl staining or H&E staining (data not shown).

Immunostaining for the glial marker GFAP (glial fibrillary acidic protein) showed increased GFAP in the hippocampal CA3 subfield of the $hrs^{loxP/loxP}$;*Synl-cre* mice, suggesting the presence of neural damage in this region (Figure 5, A and B). To determine whether the reduced number of neurons observed in the $hrs^{loxP/loxP}$;*Synl-cre* mouse brain was caused by cell death, we performed TUNEL staining, which detects the DNA fragmentation in dying cells. Several TUNEL-positive cells were detected in the hippocampal CA3 subfield of 5-week-old $hrs^{loxP/loxP}$;*Synl-cre* mice, but no TUNEL-positive cells were detected in the $hrs^{+/+}$;*Synl-cre* hippocampus (Figure 5, C and D). These results suggest that neural cell death occurs in a specific brain region of the $hrs^{loxP/loxP}$;*Synl-cre* mice, the hippocampal CA3 subfield.

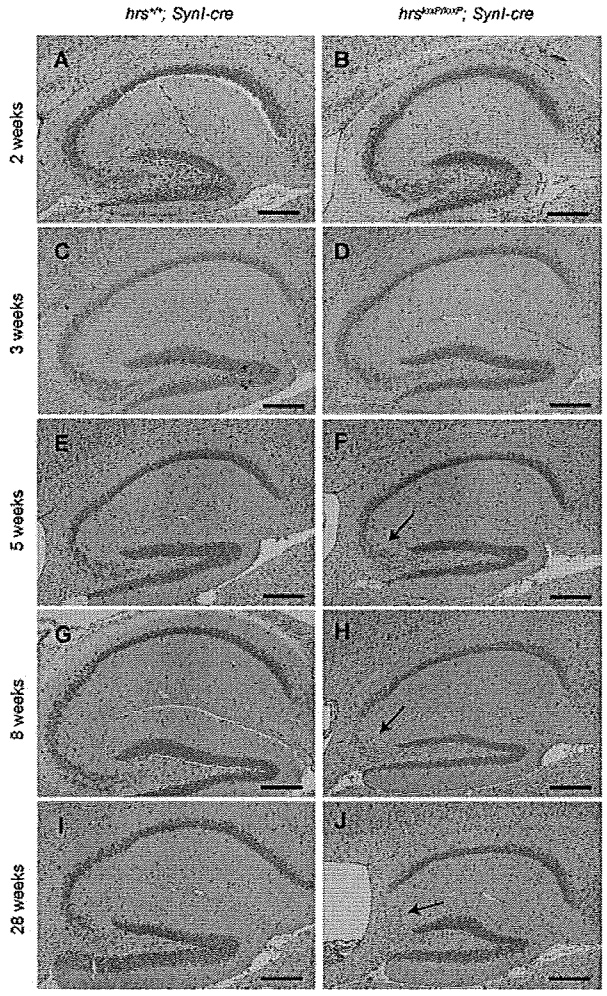

Figure 4. Abnormalities in the hippocampal CA3 subfield of *hrs*$^{loxP/loxP}$;*Synl-cre* mice. Nissl staining of anterior coronal hippocampus sections of mice. Mice were *hrs*$^{+/+}$;*Synl-cre* (**A, C, E, G, I**) and *hrs*$^{loxP/loxP}$;*Synl-cre* (**B, D, F, H, J**) and were 2 weeks (**A, B**), 3 weeks (**C, D**), 5 weeks (**E, F**), 8 weeks (**G, H**), and 28 weeks (**I, J**) of age. Note the loss of pyramidal cells in the CA3 subfield in the *hrs*$^{loxP/loxP}$;*Synl-cre* hippocampus (**arrows**). Scale bars = 250 μm. Original magnifications, ×100.

To examine the mossy fiber pathway that connects granule cells to CA3 pyramidal cells, we performed immunostaining assays for calbindin, which selectively stains neurons in the dentate gyrus containing the mossy fiber pathway and Purkinje cells. Despite the profound reduction of pyramidal cells in the hippocampal CA3 subfield of *hrs*$^{loxP/loxP}$;*Synl-cre* mice, the staining pattern of calbindin was not significantly different between the *hrs*$^{+/+}$;*Synl-cre* and *hrs*$^{loxP/loxP}$;*Synl-cre* mice (Figure 6, A and B). Immunohistochemical staining with an anti-calbindin antibody demonstrated no difference in the Purkinje cell numbers between the *hrs*$^{+/+}$;*Synl-cre* and *hrs*$^{loxP/loxP}$;*Synl-cre* mice (Figure 6, C and D).

Accumulation of Ubiquitinated Proteins in the Hrs Mutant Brain

Because Hrs has an essential role in the endocytic sorting of ubiquitinated proteins, we investigated whether

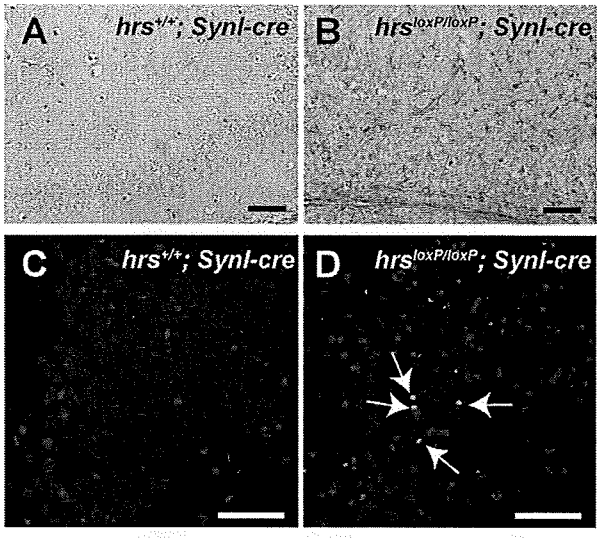

Figure 5. Neural cell death occurs in the hippocampal CA3 subfield of *hrs*$^{loxP/loxP}$;*Synl-cre* mice. **A** and **B:** Anti-GFAP antibody staining. Brain sections from *hrs*$^{+/+}$;*Synl-cre* (**A**) and *hrs*$^{loxP/loxP}$;*Synl-cre* (**B**) mice were immunostained with a GFAP-specific antibody. The GFAP signal was increased in the hippocampus of *hrs*$^{loxP/loxP}$;*Synl-cre* mice. **C** and **D:** TUNEL staining of the hippocampal CA3 subfield. Hippocampus sections of 5-week-old *hrs*$^{+/+}$;*Synl-cre* (**C**) and *hrs*$^{loxP/loxP}$;*Synl-cre* (**D**) mice were stained for TUNEL. **Arrows** indicate positive staining for TUNEL. Original magnifications, ×400. Scale bars = 50 μm.

ubiquitinated proteins accumulated in the Hrs mutant brains by immunohistochemical analysis. In the *hrs*$^{loxP/loxP}$;*Synl-cre* mouse brain, numerous granules stained by an anti-ubiquitin antibody appeared in the CA3 subfield, cerebral cortex, hypothalamus, and less frequently, in Purkinje cells (Figures 7 and 8). In the 16-week-old *hrs*$^{loxP/loxP}$;*Synl-cre* mouse brain, there were fewer ubiquitin-positive pyramidal cells, because most of the pyramidal cells were already lost (Figure 7, K–M). Interestingly, ubiquitin-positive aggregates were also observed in the 3-week-old *hrs*$^{loxP/loxP}$;*Synl-cre* mouse brain, which

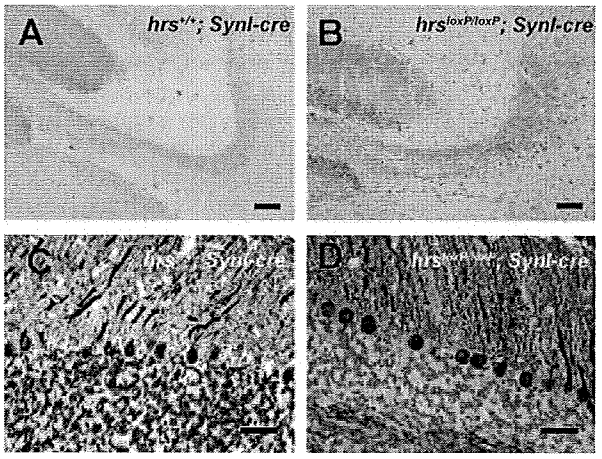

Figure 6. A and **B:** Calbindin immunostaining for mossy fibers. Sections were prepared from the brains of 8-week-old *hrs*$^{+/+}$;*Synl-cre* (**A**) and *hrs*$^{loxP/loxP}$;*Synl-cre* (**B**) mice. **C** and **D:** Calbindin immunostaining for Purkinje cells. The sections were prepared from the brains of 8-week-old *hrs*$^{+/+}$;*Synl-cre* (**C**) and *hrs*$^{loxP/loxP}$;*Synl-cre* (**D**) mice. Scale bars: 0.25 mm (**A, B**); 25 μm (**C, D**). Original magnifications: ×200 (**A, B**); ×400 (**C, D**).

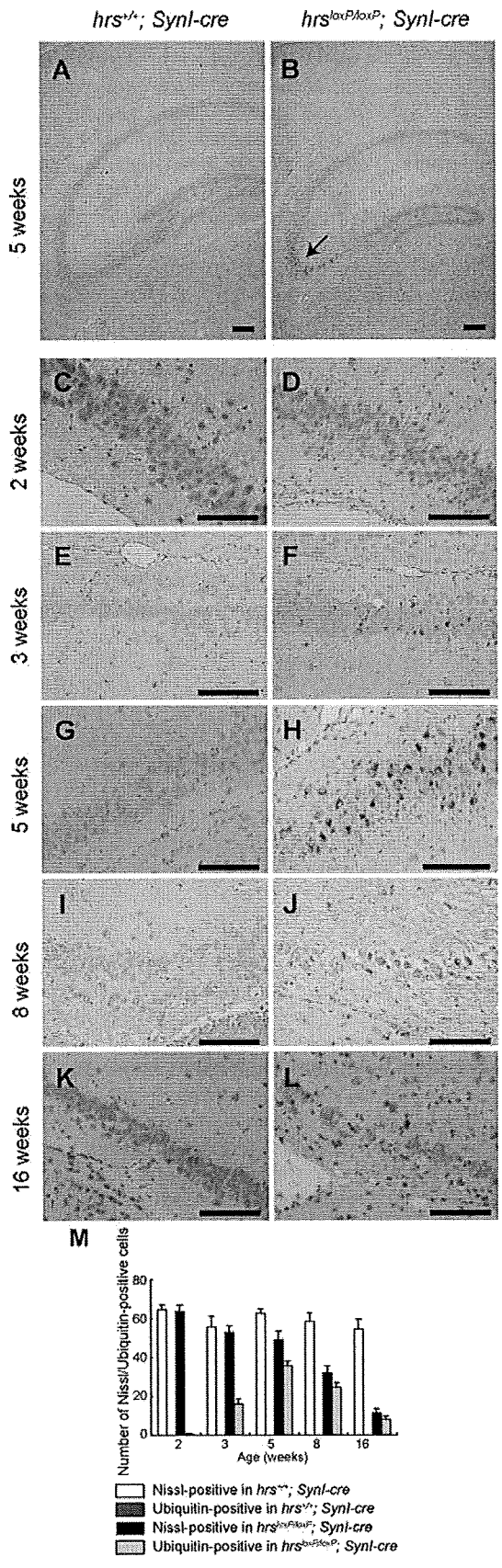

did not show the loss of hippocampal CA3 pyramidal neurons (Figure 4, C and D; and Figure 7, E, F, and M). The number of ubiquitin-positive neurons in the cerebral cortex gradually increased with age (Figure 8, A–J and O). On the other hand, we could not detect any ubiquitin-positive aggregates in the *hrs*$^{loxP/loxP}$*;MX1-cre* mouse liver, which was sufficiently knocked-out by the injection of polyriboinosinic polyribocytidylic acid (data not shown). These data suggest that Hrs plays a crucial role in the degradation of ubiquitinated proteins in neural cells.

Expression Pattern of Glutamate Receptors, PSD-95, and p62

Because Hrs binds to ubiquitinated receptors and sorts them into lysosomes through multivesicular bodies, we performed immunohistochemical analyses in the hippocampus for NR1 and NR2B, the major subunits of NR, and for GluR1, the major subunit of AMPAR. In *hrs*$^{loxP/loxP}$*;Synl-cre* mice, NR1-, NR2B-, and GluR1-positive aggregates were observed in the perikarya of CA3 pyramidal cells (Figure 9, A–L). We suspected that the PSD-95 that is abundant in virtually all mature excitatory glutaminergic synapses might also be involved in the glutamate receptor accumulation. Previous studies indicate that Hrs binds to PSD-95β[32] and that PSD-95 controls glutaminergic synapse function.[33] Nevertheless, PSD-95-positive aggregates were not detected in the *hrs*$^{loxP/loxP}$*;Synl-cre* mice (Figure 9, M–P). These data suggest that Hrs affects the degradation of NR and AMPAR without affecting PSD-95.

Because Hrs is involved in the autophagic pathway,[34] it was possible that insufficient autophagy-dependent protein degradation was the reason for the aggregation of ubiquitinated protein in the CA3 region. We therefore examined the expression of two proteins: LC3, a specific marker of autophagosomes, and p62, which is regulated by autophagy and thus accumulates when autophagy is insufficient.[35] Although LC3-positive vesicles could not be detected in either the control or Hrs mutant mouse brain (data not shown), aggregated p62 was clearly observed in the pyramidal cell perikarya in the CA3 subfield of the Hrs mutant (Figure 10, A–D). Consistent with data in Figure 7, signals detected by FK2, including mono-and polyubiquitinated proteins, were also observed in *hrs*$^{loxP/loxP}$*;Synl-cre* mice. Notably, p62, GluR1, and NR2B were co-localized with each other, as well as with the ubiquitinated proteins (Figure 10, E–L).

Figure 7. Ubiquitin-positive inclusions in the *hrs*$^{loxP/loxP}$*;Synl-cre* brain. Immunohistochemistry of hippocampal CA3 sections from *hrs*$^{+/+}$*;Synl-cre* (**A**, **C**, **E**, **G**, **I**, **K**) and *hrs*$^{loxP/loxP}$*;Synl-cre* (**B**, **D**, **F**, **H**, **J**, **L**) mice at various weeks of age, stained with an anti-ubiquitin antibody (1B3). **A** and **B:** Five weeks old, low magnification. **C** and **D:** Two weeks old. **E** and **F:** Three weeks old. **G** and **H:** Five weeks old. **I** and **J:** Eight weeks old. **K** and **L:** Sixteen weeks old. **Arrow** indicates ubiquitin-positive cells. **M:** Nissl- or ubiquitin-positive cells in the hippocampal CA3 subfield were counted in comparable areas for *hrs*$^{+/+}$*;Synl-cre* and *hrs*$^{loxP/loxP}$*;Synl-cre* mice. Data represent the mean ± SE of three mice. Scale bars = 50 μm. Original magnifications: ×100 (**A**, **B**); ×400 (**C**–**L**).

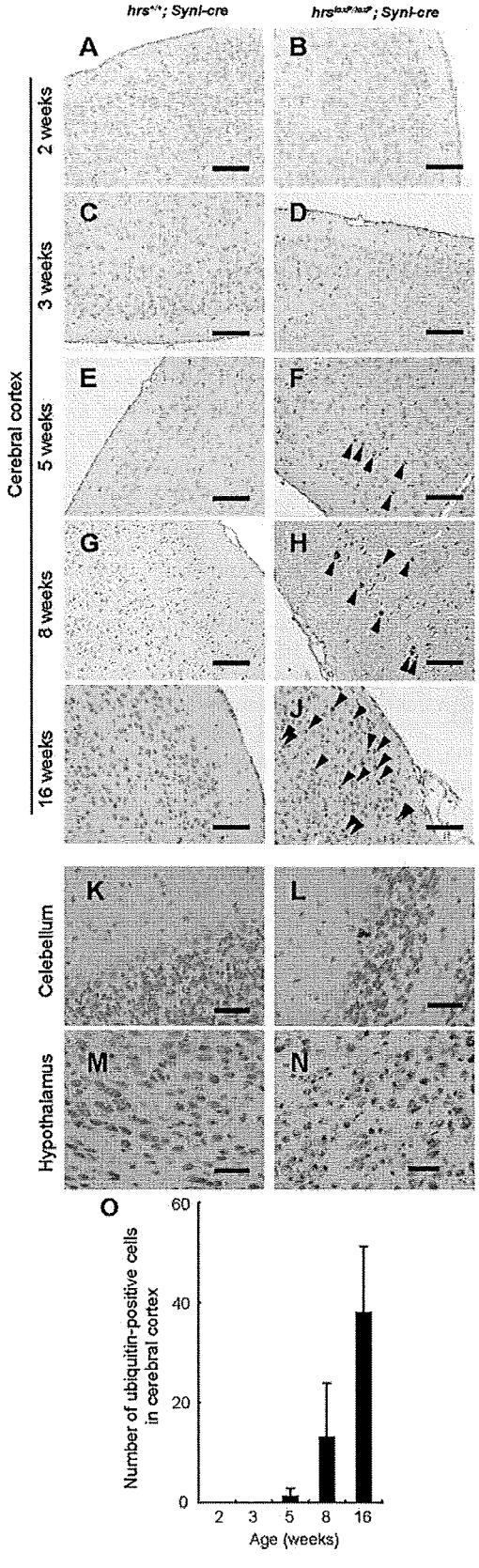

Learning Ability and Locomotor Activity Impairments in Hrs Mutant Mice

To investigate the effect of ubiquitinated protein accumulation in neural cells, behavioral analyses were performed with *hrs*$^{+/+}$*;Synl-cre* and *hrs*$^{loxP/loxP}$*;Synl-cre* mice. First, in an open field test, there were significant differences in the vertical (rearing) activity, but not in the horizontal activity, between the two groups (Figure 11, A and B). These results indicate that locomotor activity was impaired in the *hrs*$^{loxP/loxP}$*;Synl-cre* mice.

Next, because ubiquitinated proteins accumulated in the hypothalamus of the *hrs*$^{loxP/loxP}$*;Synl-cre* mice, we investigated the mental status of the two groups of mice by the forced swimming test, which is used to evaluate depression in rodents. In this test, a depressed state is induced in mice by forcing them to swim in an aquarium from which they cannot escape. The *Hrs*$^{loxP/loxP}$*;Synl-cre* mice showed a significantly longer duration of immobility (Figure 11C). To test whether *hrs*$^{loxP/loxP}$*;Synl-cre* mice had weaker muscles, we performed a wire-hanging test. No significant difference was observed between the two groups of mice in this test (Figure 11D). Footprint analysis also showed no difference between the two groups (Figure 11E). Collectively, these results indicate that the *hrs*$^{loxP/loxP}$*;Synl-cre* mice were in a depressive state.

Finally, we tested whether the loss of hippocampal CA3 neurons in the *hrs*$^{loxP/loxP}$*;Synl-cre* mice affected their learning ability. Mice were examined using a passive avoidance task. Twenty-four hours after training, the latency period for mice to enter the dark box was significantly shorter for the *hrs*$^{loxP/loxP}$*;Synl-cre* mice than for the *hrs*$^{+/+}$*;Synl-cre* mice (Figure 11F). This result is compatible with the observation of hippocampal neuron loss in the *hrs*$^{loxP/loxP}$*;Synl-cre* mice.

Discussion

In the present study, we detected the obvious accumulation of ubiquitinated proteins in 5-week-old *hrs*$^{loxP/loxP}$*;Synl-cre* brain, although neurodegeneration was not apparent in the hippocampus until after 8 weeks, suggesting that the aggregation of ubiquitinated proteins precedes neurodegeneration in these mice. We also found that ubiquitinated proteins in the cerebral cortex of *hrs*$^{loxP/loxP}$*;Synl-cre* mice increased with age, and that their learning ability was impaired, in accordance with the increase in ubiquitinated proteins. These findings reveal the importance of understanding Hrs' role in the mechanism of neurodegenerative diseases because some

Figure 8. Ubiquitin-positive inclusions in the *hrs*$^{loxP/loxP}$*;Synl-cre* brain. Immunohistochemistry of cerebral cortex (**A–J**), Purkinje cells (**K**, **L**), and hypothalamus (**M**, **N**) sections from *hrs*$^{+/+}$*;Synl-cre* (**A**, **C**, **E**, **G**, **I**, **K**, **M**) and *hrs*$^{loxP/loxP}$*;Synl-cre* (**B**, **D**, **F**, **H**, **J**, **L**, **N**) mice at various weeks of age, stained with an anti-ubiquitin antibody (1B3). **A** and **B:** Two weeks old. **C** and **D:** Three weeks old. **E**, **F**, **K**, and L: Five weeks old. **G** and **H:** Eight weeks old. **I**, **J**, **M**, and **N:** Sixteen weeks old. **Arrowheads** indicate ubiquitin-positive cells. **O:** Ubiquitin-positive cells in the cerebral cortex were counted in comparable areas for each *hrs*$^{loxP/loxP}$*;Synl-cre* mouse, and five fields were counted in each area for each mouse. Data represent the mean ± SE of three mice. Scale bars = 100 μm. Original magnifications, ×400.

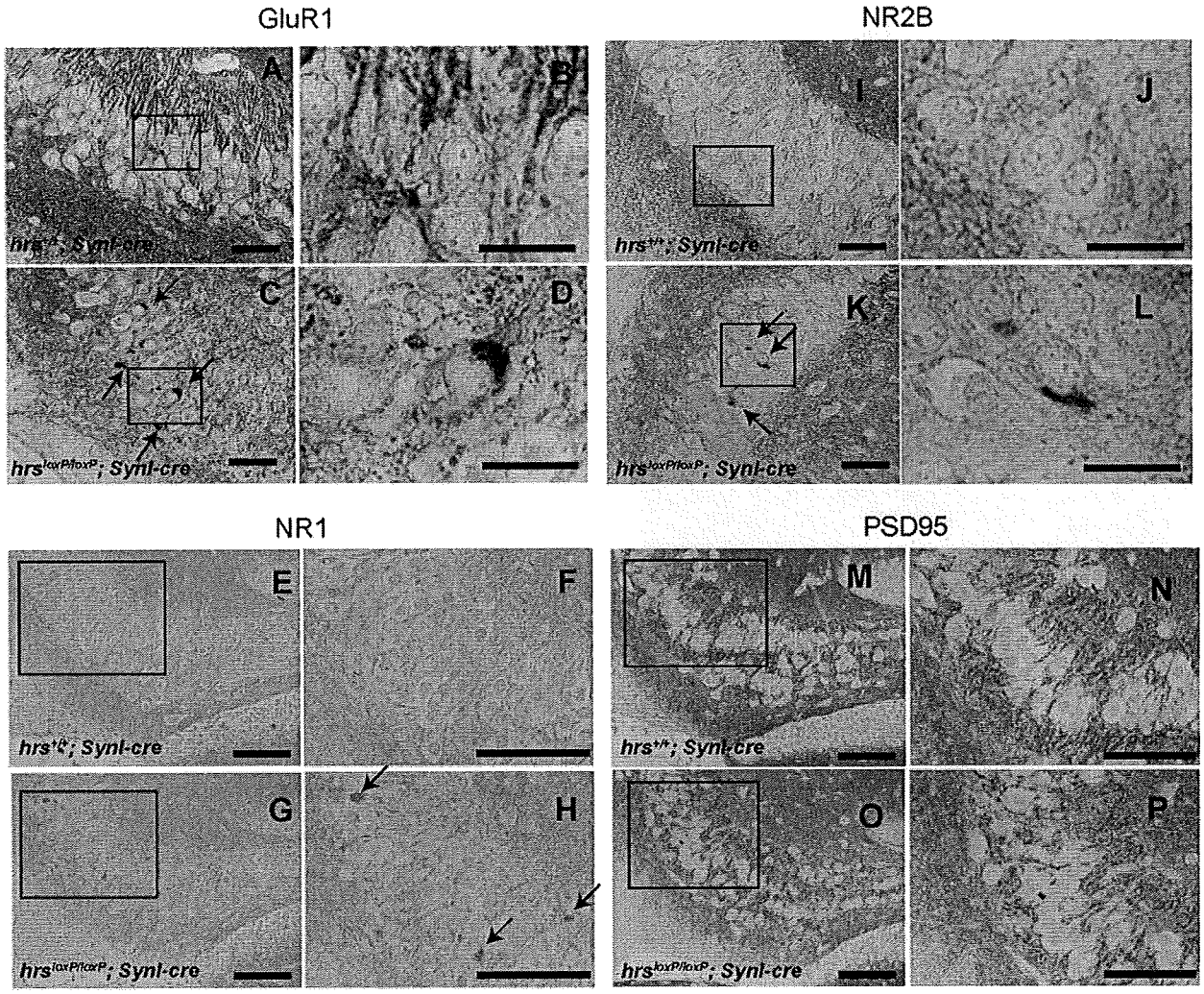

Figure 9. Immunohistochemistry of GluR1 (**A--D**), NR1 (**E–H**), NR2B (**I–L**), and PSD-95 (**M–P**) in the hippocampus CA3 subfield. Hippocampus sections from *hrs*$^{+/+}$*;Synl-cre* (**A**, **C**, **E**, **G**, **I**, **K**, **M**, **O**) and *hrs*$^{loxP/loxP}$*;Synl-cre* (**B**, **D**, **F**, **H**, **J**, **L**, **N**, **P**) 5-week-old mice were stained with GluR1-, NR1-, NR2B-, and PSD-95-specific antibodies. **Arrows** indicate protein aggregates. **Insets** show a higher magnification. Scale bars: 50 μm (**A**, **C**, **E–H**, **I**, **K**, **M–P**); 20 μm (**B**, **D**, **J**, **L**). Original magnifications, ×400.

ubiquitin-positive inclusions, such as phosphorylated tau and TDP-43, accumulate in the cerebral cortex, which results in the progressive loss of cognitive ability.[36] In this study, we could not detect the expression of phosphorylated tau in the cerebral cortex of *hrs*$^{loxP/loxP}$*;Synl-cre* mice using an anti-phosphorylated tau antibody (data not shown). Further study is required to reveal the relationship between the ESCRT proteins and neurodegenerative disease.

In neurons, NMDA receptor proteins usually concentrate at the postsynaptic density (PSD), a specialized apparatus beneath synapses that consists of receptors, scaffolding molecules, and signal-transduction enzymes. Synaptic transmission modulates the composition of the PSD, in part by the activity-dependent ubiquitination and degradation of PSD components.[37] The Mdm2-mediated ubiquitination of PSD-95 is critical for regulating the cell-surface expression of AMPA receptors in synaptic plasticity.[38] The overexpression of Hrs blocks the postsynaptic targeting of PSD-95β, which instead accumulates on large endosomal vesicles.[32] In this study, we found AMPAR- and NMDAR-positive aggregates in the hippocampus of *hrs*$^{loxP/loxP}$*;Synl-cre* mice, although their expression levels, except in the aggregates, were not significantly different between the *hrs*$^{loxP/loxP}$*;Synl-cre* and control mice. These observations suggest that the loss of hippocampal CA3 pyramidal neurons is not caused by excitotoxicity, but by protein aggregate-induced cellular toxicity. Generally, ESCRTs including Hrs were thought to regulate an endosomal pathway, not a proteasomal pathway.[11] Thus, we conclude that the loss of Hrs impairs the lysosome-dependent degradative pathway, thereby advancing the accumulation of ubiquitinated proteins, including glutamate receptors, resulting in neurodegeneration. However, we cannot exclude the possibility that we failed to detect altered CA3 pyramidal neurons in the *hrs*$^{loxP/loxP}$*;Synl-cre* mice.

Endosomes are major targets of genetic and epigenetic pathogenic factors in many neurodegenerative diseases.[39] In Huntington's disease, the expansion of a

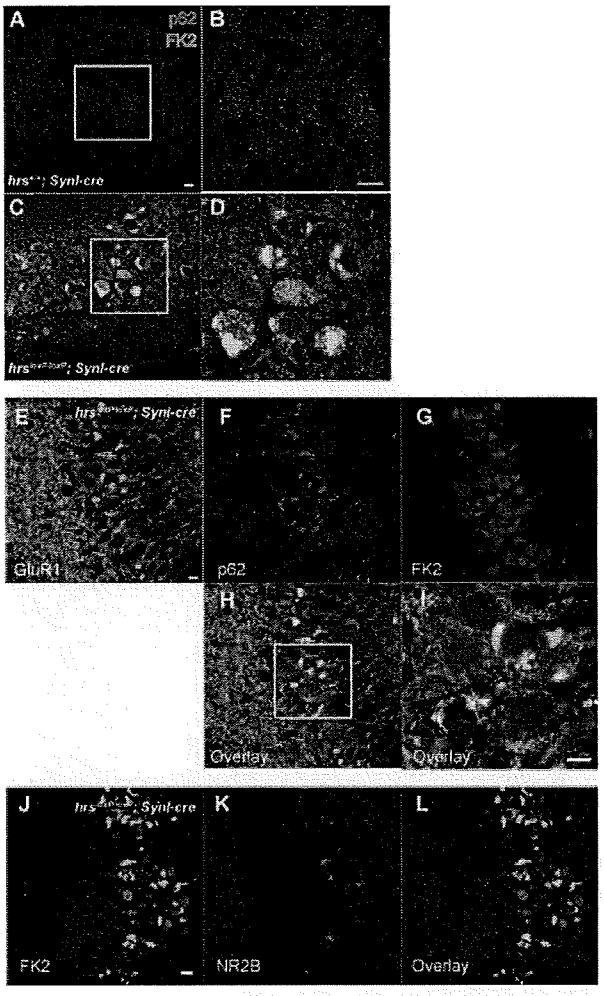

Figure 10. Immunohistochemistry of p62, FK2, GluR1, and NR2B in the hippocampus CA3 subfield. **A–D:** Aggregated p62 (red) and ubiquitinated proteins (green) were observed in the $hrs^{loxP/loxP}$;*Synl-cre* mice (**C, D**), but not in the $hrs^{+/+}$;*Synl-cre* mice (**A, B**). p62 was co-localized with ubiquitinated proteins (yellow). **E–L:** GluR1 and NR2B were also co-localized with p62 and FK2 in the $hrs^{loxP/loxP}$;*Synl-cre* mice. Scale bars = 10 μm. Original magnifications, ×400.

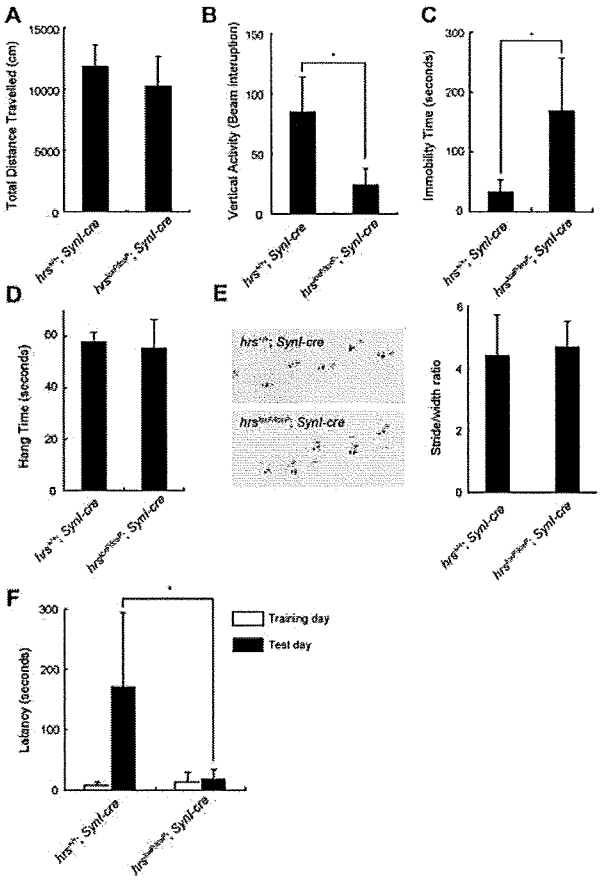

Figure 11. Behavioral examinations. **A** and **B:** The open-field activity test. Data are averages ± standard errors (n = 10) for the total distance (**A**) and vertical activity (**B**) of the $hrs^{+/+}$;*Synl-cre* and $hrs^{loxP/loxP}$;*Synl-cre* mice for 30 minutes. **C:** Increase of immobility time in the forced swimming test in the $hrs^{loxP/loxP}$;*Synl-cre* mice. Values are expressed as means ± standard errors (n = 10). **D:** Wire hanging test. $Hrs^{+/+}$;*Synl-cre* and $hrs^{loxP/loxP}$;*Synl-cre* mice were tested (n = 10). **E: Left**, paw placement records of 12-week-old mice; **right**, stride lengths corrected for paw base widths (stride/width ratio) of $hrs^{loxP/loxP}$;*Synl-cre* and $hrs^{+/+}$;*Synl-cre* littermate mice. Values are expressed as means ± standard errors of three mice. **F:** Loss of memory function of the $hrs^{loxP/loxP}$;*Synl-cre* mice in the step-through passive avoidance test. Data represent means ± standard errors of the step-through latency period (n = 10). Statistical differences between groups were determined by Student's t-test. $^*P < 0.05$.

polyglutamate tract in huntingtin (Htt) causes neuronal loss in the striatum and cortex.[40] Mutant Htt is believed to promote cell death in several ways that involve endosome dysfunction, and Htt normally associates with HIP1, a protein that co-localizes on early endosomes with its ligand Hrs.[41] Recent studies indicate that ESCRTs not only facilitate the trafficking of ubiquitylated proteins from endosomes to lysosomes, but play a critical role in autophagy; ESCRT III dysfunction causes autophagosome accumulation and neurodegeneration because of an abnormal fusion process between autophagosomes and endosomal compartments or lysosomes.[17,42] Moreover, autophagy is essential for the survival of neural cells, and its impairment is implicated in the pathogenesis of neurodegenerative disorders involving ubiquitin-containing inclusion bodies.[17,43,44] In $hrs^{loxP/loxP}$;*Synl-cre* mice, we found that ubiquitinated proteins accumulated in the hippocampus, which is similar to the finding for autophagy-deficient mice.[43,44] In this context, we previously demonstrated that Hrs plays a crucial role in autophagosome maturation.[34] Although we have not yet obtained direct evidence for it, it appears that the autophagic pathway is impaired in the hippocampal CA3 subfields of the $hrs^{loxP/loxP}$;*Synl-cre* mice, because p62, which is degraded by the autophagic pathway,[44] was among the accumulated proteins. Further study will be required to elucidate the function of Hrs in autophagy by using other organ-specific Cre transgenic mice.

It was striking that the loss of pyramidal neurons by Hrs depletion occurred only in the hippocampal CA3 subfield. It was also interesting that NR accumulated only in the CA3, and not in the CA1 subfield, even though NR1, a common subunit of NR,[45] is distributed in both CA1 and CA3. We expect that one of the following ideas will explain this selective phenotype: First, the expression of *hrs* is higher in the CA3 subfield than in CA1 (Figure 1, B and C). Second, certain cargos that are critical for neural

survival and sensitive to Hrs-dependent sorting and degradation may be restricted to CA3. Further study will be required to elucidate the reason for this specificity of Hrs-dependent neurodegeneration.

In severely depressed patients, emotional arousal, cognitive abnormality, and vulnerability to psychotic episodes are linked to hypothalamic-pituitary-adrenal axis activity.[46] Excessive stimulation of the axis is implicated in depression, and hyperactivity of the hypothalamic-pituitary-adrenal axis is observed in the majority of patients with depression.[47] We found that *hrs$^{loxP/loxP}$;Synl-cre* mice showed more immobility than controls in a forced swimming test, and that ubiquitinated proteins accumulated in the hypothalamus of these mice, although hypothalamic neurons were not lost. These observations suggest that ubiquitinated proteins in the neural cells of *hrs$^{loxP/loxP}$;Synl-cre* mice might impair hypothalamic function and the hypothalamic-pituitary-adrenal axis. We also found that the loss of Hrs markedly impaired the retention of passive avoidance behavior 24 hours after the training trial. A previous study showed that CA3 NMDAR function is absent during memory formation in CA3-NR1 KO mice,[48] which is similar to the phenotype of Hrs mutant mice. Our data are compatible with this study.

The present study indicates that Hrs plays a pivotal role in the survival of neural cells through its involvement in the degradation pathway for ubiquitinated proteins. Although it is still unknown whether Hrs selectively recognizes harmful gene products associated with neurodegenerative disorders such as Huntington's, Parkinson's, and Alzheimer's disease, our Hrs mutant mice provide an excellent animal model system for studying the molecular mechanisms of neurodegenerative diseases.

Acknowledgments

We thank Dr. Jamey D. Marth for the Synapsin-I Cre transgenic mice; Kazuhiko Yanai and Eiko Sakurai for their help with the behavioral examinations; Drs. Hiromu Yawo, Yasuto Itoyama, Ichiro Sora, and Toshio Watanabe for discussion; and Ms. Rie Ito for technical assistance.

References

1. Ballatore C, Lee VM, Trojanowski JQ: Tau-mediated neurodegeneration in Alzheimer's disease and related disorders. Nat Rev Neurosci 2007, 8:663–672
2. Trojanowski JQ, Lee VM: "Fatal attractions" of proteins: a comprehensive hypothetical mechanism underlying Alzheimer's disease and other neurodegenerative disorders. Ann N Y Acad Sci 2000, 924:62–67
3. Rubinsztein DC: The roles of intracellular protein-degradation pathways in neurodegeneration. Nature 2006, 443:780–786
4. Aarts MM, Tymianski M: Molecular mechanisms underlying specificity of excitotoxic signaling in neurons. Curr Mol Med 2004, 4:137–147
5. Mattson MP: Excitotoxic and excitoprotective mechanisms: abundant targets for the prevention and treatment of neurodegenerative disorders. Neuromolecular Med 2003, 3:65–94
6. Moghaddam B: Bringing order to the glutamate chaos in schizophrenia. Neuron 2003, 40:881–884
7. Tzschentke TM: Glutamatergic mechanisms in different disease states: overview and therapeutical implications—an introduction. Amino Acids 2002, 23:147–152
8. Mori H, Mishina M: Structure and function of the NMDA receptor channel. Neuropharmacology 1995, 34:1219–1237
9. Kato A, Rouach N, Nicoll RA, Bredt DS: Activity-dependent NMDA receptor degradation mediated by retrotranslocation and ubiquitination. Proc Natl Acad Sci USA 2005, 102:5600–5605
10. Schaefer H, Rongo C: KEL-8 is a substrate receptor for CUL3-dependent ubiquitin ligase that regulates synaptic glutamate receptor turnover. Mol Biol Cell 2006, 17:1250–1260
11. Babst M: A protein's final ESCRT. Traffic 2005, 6:2–9
12. Raiborg C, Rusten TE, Stenmark H: Protein sorting into multivesicular endosomes. Curr Opin Cell Biol 2003, 15:446–455
13. Komada M, Soriano P: Hrs, a FYVE finger protein localized to early endosomes, is implicated in vesicular traffic and required for ventral folding morphogenesis. Genes Dev 1999, 13:1475–1485
14. Miura S, Takeshita T, Asao H, Kimura Y, Murata K, Sasaki Y, Hanai JI, Beppu H, Tsukazaki T, Wrana JL, Miyazono K, Sugamura K: Hgs (Hrs), a FYVE domain protein, is involved in Smad signaling through cooperation with SARA. Mol Cell Biol 2000, 20:9346–9355
15. Ehlers MD: Deconstructing the axon: Wallerian degeneration and the ubiquitin-proteasome system. Trends Neurosci 2004, 27:3–6
16. Filimonenko M, Stuffers S, Raiborg C, Yamamoto A, Malerod L, Fisher EM, Isaacs A, Brech A, Stenmark H, Simonsen A: Functional multivesicular bodies are required for autophagic clearance of protein aggregates associated with neurodegenerative disease. J Cell Biol 2007, 179:485–500
17. Lee JA, Beigneux A, Ahmad ST, Young SG, Gao FB: ESCRT-III dysfunction causes autophagosome accumulation and neurodegeneration. Curr Biol 2007, 17:1561–1567
18. Yagi T, Tokunaga T, Furuta Y, Nada S, Yoshida M, Tsukada T, Saga Y, Takeda N, Ikawa Y, Aizawa S: A novel ES cell line, TT2, with high germline-differentiating potency. Anal Biochem 1993, 214:70–76
19. Dymecki SM: Flp recombinase promotes site-specific DNA recombination in embryonic stem cells and transgenic mice. Proc Natl Acad Sci USA 1996, 93:6191–6196
20. Zhu Y, Romero MI, Ghosh P, Ye Z, Charnay P, Rushing EJ, Marth JD, Parada LF: Ablation of NF1 function in neurons induces abnormal development of cerebral cortex and reactive gliosis in the brain. Genes Dev 2001, 15:859–876
21. Tanaka N, Kaneko K, Asao H, Kasai H, Endo Y, Fujita T, Takeshita T, Sugamura K: Possible involvement of a novel STAM-associated molecule "AMSH" in intracellular signal transduction mediated by cytokines. J Biol Chem 1999, 274:19129–19135
22. Asao H, Sasaki Y, Arita T, Tanaka N, Endo K, Kasai H, Takeshita T, Endo Y, Fujita T, Sugamura K: Hrs is associated with STAM, a signal-transducing adaptor molecule. Its suppressive effect on cytokine-induced cell growth. J Biol Chem 1997, 272:32785–32791
23. Abe M, Fukaya M, Yagi T, Mishina M, Watanabe M, Sakimura K: NMDA receptor GluRepsilon/NR2 subunits are essential for postsynaptic localization and protein stability of GluRzeta1/NR1 subunit. J Neurosci 2004, 24:7292–7304
24. Fukaya M, Kato A, Lovett C, Tonegawa S, Watanabe M: Retention of NMDA receptor NR2 subunits in the lumen of endoplasmic reticulum in targeted NR1 knockout mice. Proc Natl Acad Sci USA 2003, 100:4855–4860
25. Nagy GG, Al-Ayyan M, Andrew D, Fukaya M, Watanabe M, Todd AJ: Widespread expression of the AMPA receptor GluR2 subunit at glutamatergic synapses in the rat spinal cord and phosphorylation of GluR1 in response to noxious stimulation revealed with an antigen-unmasking method. J Neurosci 2004, 24:5766–5777
26. Yamada M, Takeshita T, Miura S, Murata K, Kimura Y, Ishii N, Nose M, Sakagami H, Kondo H, Tashiro F, Miyazaki JI, Sasaki H, Sugamura K: Loss of hippocampal CA3 pyramidal neurons in mice lacking STAM1. Mol Cell Biol 2001, 21:3807–3819
27. Schaeren-Wiemers N, Gerfin-Moser A: A single protocol to detect transcripts of various types and expression levels in neural tissue and cultured cells: in situ hybridization using digoxigenin-labelled cRNA probes. Histochemistry 1993, 100:431–440
28. Chen Z, Sakurai E, Hu W, Jin C, Kiso Y, Kato M, Watanabe T, Wei E, Yanai K: Pharmacological effects of carcinine on histaminergic neurons in the brain. Br J Pharmacol 2004, 143:573–580
29. Sango K, McDonald MP, Crawley JN, Mack ML, Tifft CJ, Skop E, Starr CM, Hoffmann A, Sandhoff K, Suzuki K, Proia RL: Mice lacking both

subunits of lysosomal beta-hexosaminidase display gangliosidosis and mucopolysaccharidosis. Nat Genet 1996, 14:348–352
30. Zomkowski AD, Santos AR, Rodrigues AL: Putrescine produces antidepressant-like effects in the forced swimming test and in the tail suspension test in mice. Prog Neuropsychopharmacol Biol Psychiatry 2006, 30:1419–1425
31. Klapdor K, Dulfer BG, Hammann A, Van der Staay FJ: A low-cost method to analyse footprint patterns. J Neurosci Methods 1997, 75:49–54
32. Chetkovich DM, Bunn RC, Kuo SH, Kawasaki Y, Kohwi M, Bredt DS: Postsynaptic targeting of alternative postsynaptic density-95 isoforms by distinct mechanisms. J Neurosci 2002, 22:6415–6425
33. Béique JC, Lin DT, Kang MG, Aizawa H, Takamiya K, Huganir RL: Synapse-specific regulation of AMPA receptor function by PSD-95. Proc Natl Acad Sci USA 2006, 103:19535–19540
34. Tamai K, Tanaka N, Nara A, Yamamoto A, Nakagawa I, Yoshimori T, Ueno Y, Shimosegawa T, Sugamura K: Role of Hrs in maturation of autophagosomes in mammalian cells. Biochem Biophys Res Commun 2007, 360:721–727
35. Komatsu M, Waguri S, Koike M, Sou YS, Ueno T, Hara T, Mizushima N, Iwata J, Ezaki J, Murata S, Hamazaki J, Nishito Y, Iemura S, Natsume T, Yanagawa T, Uwayama J, Warabi E, Yoshida H, Ishii T, Kobayashi A, Yamamoto M, Yue Z, Uchiyama Y, Kominami E, Tanaka K: Homeostatic levels of p62 control cytoplasmic inclusion body formation in autophagy-deficient mice. Cell 2007, 131:1149–1163
36. Forman MS, Trojanowski JQ, Lee VM: Neurodegenerative diseases: a decade of discoveries paves the way for therapeutic breakthroughs. Nat Med 2004, 10:1055–1063
37. Ehlers MD: Activity level controls postsynaptic composition and signaling via the ubiquitin-proteasome system. Nat Neurosci 2003, 6:231–242
38. Colledge M, Snyder EM, Crozier RA, Soderling JA, Jin Y, Langeberg LK, Lu H, Bear MF, Scott JD: Ubiquitination regulates PSD-95 degradation and AMPA receptor surface expression. Neuron 2003, 40:595–607
39. Nixon RA: Endosome function and dysfunction in Alzheimer's disease and other neurodegenerative diseases. Neurobiol Aging 2005, 26:373–382
40. Vonsattel JP, DiFiglia M: Huntington disease. J Neuropathol Exp Neurol 1998, 57:369–384
41. Metzler M, Li B, Gan L, Georgiou J, Gutekunst CA, Wang Y, Torre E, Devon RS, Oh R, Legendre-Guillemin V, Rich M, Alvarez C, Gertsenstein M, McPherson PS, Nagy A, Wang YT, Roder JC, Raymond LA, Hayden MR: Disruption of the endocytic protein HIP1 results in neurological deficits and decreased AMPA receptor trafficking. EMBO J 2003, 22:3254–3266
42. Rusten TE, Vaccari T, Lindmo K, Rodahl LM, Nezis IP, Sem-Jacobsen C, Wendler F, Vincent JP, Brech A, Bilder D, Stenmark H: ESCRTs and Fab1 regulate distinct steps of autophagy. Curr Biol 2007, 17:1817–1825
43. Hara T, Nakamura K, Matsui M, Yamamoto A, Nakahara Y, Suzuki-Migishima R, Yokoyama M, Mishima K, Saito I, Okano H, Mizushima N: Suppression of basal autophagy in neural cells causes neurodegenerative disease in mice. Nature 2006, 441:885–889
44. Komatsu M, Waguri S, Chiba T, Murata S, Iwata J, Tanida I, Ueno T, Koike M, Uchiyama Y, Kominami E, Tanaka K: Loss of autophagy in the central nervous system causes neurodegeneration in mice. Nature 2006, 441:880–884
45. Köhr G: NMDA receptor function: subunit composition versus spatial distribution. Cell Tissue Res 2006, 326:439–446
46. de Kloet ER, Derijk RH, Meijer OC: Therapy insight: is there an imbalanced response of mineralocorticoid and glucocorticoid receptors in depression? Nat Clin Pract Endocrinol Metab 2007, 3:168–179
47. Berton O, Nestler EJ: New approaches to antidepressant drug discovery: beyond monoamines. Nat Rev Neurosci 2006, 7:137–151
48. Nakazawa K, Quirk MC, Chitwood RA, Watanabe M, Yeckel MF, Sun LD, Kato A, Carr CA, Johnston D, Wilson MA, Tonegawa S: Requirement for hippocampal CA3 NMDA receptors in associative memory recall. Science 2002, 297:211–218

Association of Gankyrin Protein Expression with Early Clinical Stages and Insulin-Like Growth Factor-Binding Protein 5 Expression in Human Hepatocellular Carcinoma

Atsushi Umemura,[1,2] Yoshito Itoh,[2] Katsuhiko Itoh,[1] Kanji Yamaguchi,[2] Tomoki Nakajima,[2] Hiroaki Higashitsuji,[1] Hitoshi Onoue,[3] Manabu Fukumoto,[4] Takeshi Okanoue,[2] and Jun Fujita[1]

Gankyrin (also known as PSMD10) is a liver oncoprotein that interacts with multiple proteins including MDM2 and accelerates degradation of the tumor suppressors p53 and Rb. We produced a monoclonal anti-gankyrin antibody and immunohistochemically assessed the clinicopathological significance of gankyrin overexpression in 43 specimens of human hepatocellular carcinoma (HCC). Specific cytoplasmic staining for gankyrin was observed in 62.8% (27/43) of HCCs, which was significantly associated with low TNM stage ($P = 0.004$), no capsular invasion ($P = 0.018$), no portal venous invasion ($P = 0.008$), and no intrahepatic metastasis ($P = 0.012$). The cumulative survival rate of patients with gankyrin-positive HCC was significantly higher than that with gankyrin-negative HCC ($P = 0.037$). p53 and MDM2 were positively stained by antibodies in 30.2% and 23.3%, respectively, of HCCs, but neither was inversely associated with gankyrin expression. In the Huh-7 human HCC cell line, overexpression of gankyrin up-regulated expression of insulin-like growth factor binding protein 5 (IGFBP-5), whereas suppression of gankyrin expression by siRNA down-regulated it. Supression of IGFBP-5 expression inhibited proliferation of Huh-7 cells as well as U-2 OS osteosarcoma cells. In HCC specimens, positive staining for IGFBP-5 was observed by immunohistochemistry in 41.9% (18/43), and the level of expression was significantly correlated with that of gankyrin ($rho = 0.629$, $P < 0.001$). *Conclusion:* These results suggest that gankyrin plays an oncogenic role(s) mainly at the early stages of human hepatocarcinogenesis, and that IGFBP-5 inducible by gankyrin overexpression may be involved in it. (HEPATOLOGY 2008;47:493-502.)

Liver cancer is the sixth most common cancer worldwide (626,000 or 5.7% of new cancer cases) and the third most common cause of death from cancer (598,000) in 2002.[1] Eighty-two percent of cases are in developing countries, and the areas of high incidence are sub-Saharan Africa, eastern and southeastern Asia, and Melanesia. Histologically, more than 90% of the primary liver cancers are hepatocellular carcinomas (HCCs). Although there are several modalities of treatment for HCC, most patients present with unresectable tumors, and nonsurgical treatments are minimally effective at best.[2,3] Even for those patients who undergo surgical resection, the recurrence rate is very high and the prognosis is poor.[2,4-6] It is therefore important to clarify the mechanisms of human hepatocarcinogenesis and identify molecular targets to develop novel diagnostic, therapeutic, and preventive strategies.

By constructing subtracted complementary DNA (cDNA) libraries, we have previously identified 19 genes overexpressed in HCCs including 2 novel genes.[7,8] One of them was named gankyrin (gann-ankyrin repeat pro-

Abbreviations: 3A6C2, mouse monoclonal anti-gankyrin antibody; cDNA, complementary DNA; HCC, hepatocellular carcinoma; IGF, insulinlike growth factor; IGFBP-5, insulin-like growth factor-binding protein 5; MDM2, mouse double minute 2; mRNA, messenger RNA; RT-PCR, reverse transcription polymerase chain reaction; siRNA, short interfering RNA; TNM, tumor-node-metastasis.

From the [1]Department of Clinical Molecular Biology, Graduate School of Medicine, Kyoto University, Kyoto, Japan; the [2]Molecular Gastroenterology and Hepatology, Graduate School of Medical Science, Kyoto Prefectural University of Medicine, Kyoto, Japan; the [3]Department of Nutritional Science, Faculty of Health and Welfare, Seinan Jo Gakuin University, Kitakyushu, Japan; and the [4]Department of Pathology, Institute of Development, Aging, and Cancer, Tohoku University, Sendai, Japan

Received May 21, 2007; accepted September 3, 2007.

Supported by Grants-in aid from the Ministry of Education, Culture, Sports, Science, and Technology of Japan and the Japan Society for the Promotion of Science.

Address reprint requests to: Jun Fujita, Department of Clinical Molecular Biology, Graduate School of Medicine, Kyoto University, 54 Shogoin Kawaharacho, Sakyo-ku, Kyoto 606-8507, Japan. E-mail: jfujita@virus.kyoto-u.ac.jp; fax: (81) 75-751-4977.

Published online in Wiley InterScience (www.interscience.wiley.com).

DOI 10.1002/hep.22027

Potential conflict of interest: Nothing to report.

tein; "gann" in Japanese means cancer).[9] Gankyrin (also called PSMD10) consists of 7 ankyrin repeats, and its messenger RNA (mRNA) was overexpressed in 34 of 34 HCCs analyzed.[9,10] Independently, gankyrin was isolated as the p28 component or the interactor of the S6b subunit of the 19S regulator of the 26S proteasome.[11,12] The ankyrin repeat is the functional domain involved in protein–protein interactions, and gankyrin has been shown to interact with multiple proteins in addition to S6b. Gankyrin binds to retinoblastoma protein (Rb) and cyclin-dependent kinase (Cdk4), and accelerates phosphorylation and degradation of Rb, which results in release of the E2F transcription factor to activate DNA synthesis genes.[9,13] Gankyrin seems to play a role in cell cycle progression in noncancerous cells as well. Overexpression of gankyrin shortens population doubling time of NIH/3T3 mouse fibroblasts,[9] and its up-regulation correlates with cell cycle progression in normal rat primary hepatocytes, oval cells, and human hepatocytes.[14,15]

Overexpression of gankyrin confers tumorigenicity to NIH/3T3 cells and inhibits apoptosis in cultured human tumor cells exposed to chemotherapeutic agents.[10] The anti-apoptotic activity is attributable, at least partly, to increased degradation of p53, resulting in the reduced transcription of the p53-dependent proapoptotic genes.[16] Gankyrin binds to the E3 ubiquitin ligase MDM2 *in vitro* and *in vivo,* which increases p53–MDM2 association, thereby facilitating the ubiquitination and subsequent proteasomal degradation of p53 by MDM2. Gankyrin also controls MDM2 auto-ubiquitination and degradation, especially in the absence of p53.[16]

We produced a mouse monoclonal antibody against human gankyrin and assessed the expression of gankyrin protein in surgically resected HCC specimens by immunohistochemistry. Correlation of gankyrin positivity with clinicopathological findings and expression of p53 and MDM2 in HCC was analyzed. Furthermore, we demonstrated that expression of insulin-like growth factor-binding protein 5 (IGFBP-5) is inducible by overexpression of gankyrin in HCCs.

Patients and Methods

Patients and Specimens. HCC tissues and their corresponding noncancerous liver tissues were obtained from 43 and 32 patients, respectively, who had undergone curative hepatectomy at the University Hospital of Kyoto Prefectural University of Medicine between 1992 and 2000. The specimens used were routinely processed, formalin-fixed, and paraffin-embedded. After hematoxylin-eosin staining, all samples were diagnosed as HCC and the tumor-node-metastasis (TNM) classification was made according to the fourth edition of the general rules for the clinical and pathological study of primary liver cancer proposed by the Liver Cancer Study Group of Japan.[17] The demographic profiles of the patients are summarized in Table 1. For western blot analysis, HCCs and noncancerous liver tissues were obtained from 3 patients undergoing liver transplantation at the University Hospital of Kyoto Prefectural University of Medicine between 2004 and 2006. No donor organs were obtained from executed prisoners or other institutionalized persons. The study protocol conformed to the ethical guidelines of the 1975 Declaration of Helsinki and was approved by the institutional review boards. Written informed consents were obtained from all patients for subsequent use of their resected tissues.

Table 1. Patient and Tumor Characteristics

Characteristic	Number (Percentage)
Number of patients	43
Sex distribution	
Male	27 (62.8%)
Female	16 (37.2%)
Age (years)	25-78, median 65
Virus marker	
HBV(+)/HCV(−)	6 (14.0%)
HBV(−)/HCV(+)	28 (65.0%)
HBV(+)/HCV(+)	3 (7.0%)
HBV(−)/HCV(−)	6 (14.0%)
AFP(ng/mL)	3.5-39999, median 90
Tumor size (cm)	1.6-17.0, median 4.0
Liver cirrhosis	
Yes	29 (67.5%)
No	14 (32.5%)
Chronic hepatitis	13 (30.2%)
Normal	1 (2.3%)
TNM stage	
I	4 (9.3%)
II	22 (51.1%)
III	8 (18.6%)
IV	9 (21.0%)
Histological differentiation	
Well	12 (27.9%)
Moderate	25 (58.1%)
Poor	6 (14.0%)
Capsular formation	
Yes	36 (83.7%)
No	7 (16.3%)
Capsular invasion	
Yes	14 (32.6%)
No	29 (67.4%)
Portal venous invasion	
Yes	9 (20.9%)
No	34 (79.1%)
Intrahepatic metastasis	
Yes	16 (37.2%)
No	27 (62.8%)

Abbreviations: HCV(+), anti-hepatitis C virus antibody positive; HBV(+), hepatitis B surface antigen positive; (−), negative; AFP, serum alpha-fetoprotein.

Cell Culture and Transfection. Huh-7 human HCC cells, U-2 OS human osteosarcoma cells, 293T human embryonic kidney cells, mouse lymph node cells, and P3X63Ag8U.1 mouse myeloma cells were cultured in Dulbecco's modified Eagle's medium (Gibco BRL Life Technologies, NY) supplemented with 10% fetal bovine serum as described.[16] To assess viable cell numbers, we used the Dojindo Cell Counting Kit-8 (CCK8 kit, Dojindo Laboratories, Kumamoto, Japan) according to the manufacturer's instructions.

The 293T, Huh-7, and U-2 OS cells were transfected with plasmid DNA by using the calcium phosphate method or FuGENE 6 Transfection Reagent (Roche Diagnostics, Mannheim, Germany) as described.[16] Short interfering RNA (siRNA) were transfected at a final concentration of 25 nM by using siPORT NeoFX Transfection Agent (Ambion, Austin, TX) following the manufacturer's instructions. Twenty-four hours after transfection, the medium was replaced with fresh medium containing fetal bovine serum, and the culture was continued for another 24 or 48 hours. Then, the cells were harvested for analysis. All transfection assays were repeated at least 3 times.

Plasmids and siRNA. Human wild-type gankyrin cDNAs, full coding sequence and deletion mutants, were cloned into the mammalian expression vector pMKIT-NEO and expressed as hemagglutinin (HA)-tagged proteins (Fig. 1A). Full-length gankyrin was expressed without a tag as well. To obtain recombinant human gankyrin protein, the full-length cDNA was cloned into an expression vector derived from pET28 (Novagen, EMD Biosciences Inc., San Diego, CA) and expressed as hexahistidine-tagged protein.

To down-regulate gene expression, Silencer Predesigned siRNAs for gankyrin (Ambion) and Stealth Select iRNA: for IGFBP-5 (Invitrogen, Tokyo, Japan), were used together with respective control RNAs.

Antibodies. To obtain monoclonal antibodies against human gankyrin, recombinant (His)6-gankyrin protein was used as an immunogen. It was dissolved in phosphate-buffered saline (1 mg/mL) and emulsified with an equal volume of Freund's complete adjuvant (Difco, Becton-Dickinson, Franklin Lakes, NJ). Two female BALB/c mice were injected with the emulsion (50 μL/mouse) in the footpad. Two weeks after immunization, the inguinal lymph node cells (4×10^7 cells) were fused with P3X63Ag8U.1 myeloma cells (1×10^7) using polyethylene glycol 1500 (Roche Diagnostics). Fused cells were cultured in 96-well plates at 2×10^5 cell/well. The supernatants were assayed for the anti-gankyrin antibody titer by an enzyme-linked immunosorbent assay using recombinant His-tagged, glutathione-S-transferase (GST)-tagged, and nontagged gankyrin proteins. Selected relevant hybridomas were cloned by the limiting dilution method, and the isotypes of secreted monoclonal antibodies were determined by the IsoStrip kit (Roche Diagnostics) following the manufacturer's instructions. Finally, an IgG2b kappa monoclonal antibody that showed the highest affinity for gankyrin was obtained and named 3A6C2.

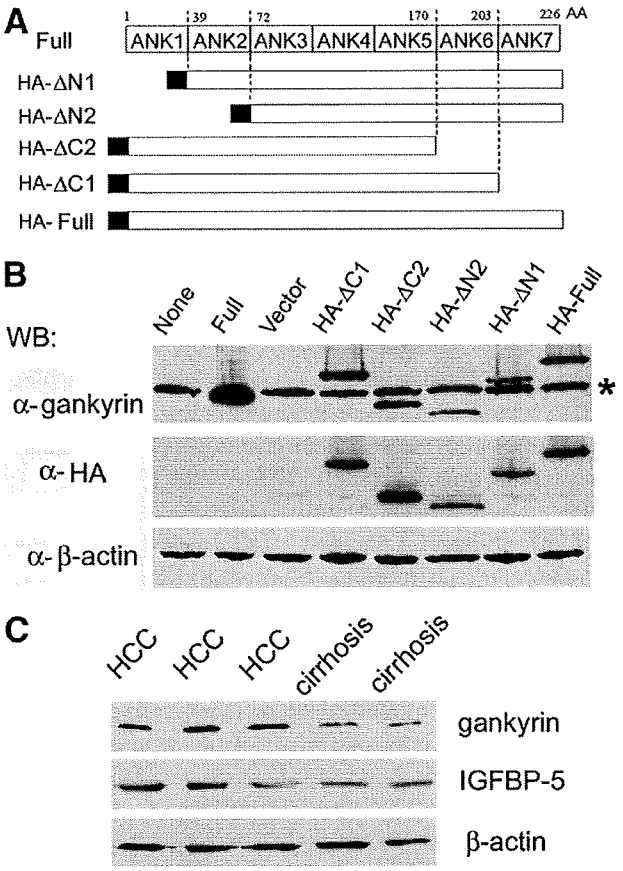

Fig. 1. Recognition of gankyrin protein by the monoclonal antibody. (A) Structures of wild-type gankyrin (Full) and its deletion mutants. Numbers on top, N- and C-terminal amino-acid residues. ANK, ankyrin repeat. Black bars, HA tags. (B) Specificity of the antibody. 293T cells were transfected with plasmids expressing the indicated proteins. Cell lysates were analyzed by western blotting (WB) using the anti-gankyrin monoclonal antibody (3A6C2), anti-HA antibody, and anti-β-actin antibody. *Mobility of the endogenous gankyrin. Representative results of 3 repeated experiments are shown. (C) Detection of gankyrin protein in tissues. Lysates were made from hepatocellular carcinoma (HCC, n = 3) and cirrhotic liver tissues (n = 2), and analyzed by WB using antibodies for indicated proteins. HA, hemagglutinin.

For western blot analysis, mouse monoclonal anti-gankyrin antibody (3A6C2), goat polyclonal anti–IGFBP-5 antibody (R&D Systems Inc., Minneapolis, MN), mouse monoclonal anti-HA antibody (12CA5, Roche Diagnostics), and mouse monoclonal anti–β-actin antibody (Chemicon International, Temecula, CA) were

used. Horseradish peroxidase–conjugated secondary antibodies against mouse or goat immunoglobulins were obtained from DAKO (Kyoto, Japan).

For immunohistochemistry, mouse monoclonal anti-gankyrin (3A6C2), anti-MDM2 (Ab-4, Oncogene research products, Boston, MA), and anti-p53 (DO-7, DAKO) antibodies, rabbit polyclonal anti-IGFBP-5 antibody (GroPep, Thebarton, Australia), and horseradish peroxidase–conjugated secondary antibodies against mouse or rabbit immunoglobulins (DAKO) were used.

Analysis of Gene Expression. Extraction of RNA, preparation of cell and tissue lysates, and western blot analysis were performed as described.[9] Real-time reverse transcription polymerase chain reaction (RT-PCR) analysis was performed using ABI PRISM 7900 (Applied Biosystems, Foster City, CA) and a 1-step QuantiTect RT-PCR Kit (Qiagen, Cowley, UK) according to the manufacturer's instructions. PCR conditions were 50°C for 30 minutes and 95°C for 15 minutes, followed by 45 cycles of 95°C for 15 seconds, 55°C for 30 seconds, and 72°C for 45 seconds. Specific PCR amplification products were detected by SYBR Green. Transcripts of β-actin were quantified as control. Primer sequences used were as follows: IGFBP-5, AAGAAGCTGACCCAGTCCAA and GAATCCTTTGCGGTCACAAT; gankyrin, GCAACTTGGAGTGCCAGTGAA and TCACTTGAGCACCTTTTCCCA; β-actin, CTACGTCGCCCTGGACTTCGAGC and GATGGAGCCGCCGATCCACACGG.

The immunohistochemical staining was performed on 4-μm-thick paraffin sections of tissues fixed in buffered formalin. The sections were pretreated with 10 mM citrate buffer (pH 6.1) in a microwave oven for 5 minutes. Endogenous peroxidase activity was blocked with 0.3 % H_2O_2 for 10 minutes. The sections were incubated with 10% fetal bovine serum for 30 minutes to reduce nonspecific binding, followed by incubation with the primary antibody at 4°C overnight. They were subsequently incubated with horseradish peroxidase–conjugated anti-mouse or rabbit immunoglobulin antibody for 30 minutes. The enzymatic reaction was developed in a freshly prepared solution of 3,3′-diaminobenzidine tetrahydrochloride using DAKO Liquid DAB Substrate-Chromogen Solution for 10 minutes at room temperature. The sections were then counterstained with hematoxylin. The staining pattern, the distribution of the immunostaining in each tissue, and the intensity of the staining were studied in detail. Negative controls were conducted by substituting normal sera of each animal for the primary antibodies. When immunoreactivities were heterogenously observed, cases with moderate or strong staining of nucleus or cytoplasm in more than 5% of the cells were considered positive. To analyze the correlation of the expression levels of gankyrin and IGFBP-5, the staining intensity was expressed as 0 (negative), 1+ (weakly positive), 2+ (moderately positive), or 3+ (strongly positive). In each case the immunoreactivity was determined in 5 random high-powered fields and the count was done independently by 2 observers.

Statistical Analysis. Categorical variables were compared using Fisher's exact test. Paired comparison of continuous data was performed using the Wilcoxon signed ranks test. To assess whether the 2 variables covary, Spearman's rank correlation coefficient was determined. Cumulative survival curves were calculated by the Kaplan-Meier method and analyzed by the log-rank test. All statistical analyses were performed using the JMP statistical software package (SAS Institute Inc., Cary, NC). A P value less than 0.05 was considered statistically significant.

Results

Clinicopathological Profiles. Forty-three patients with HCC were recruited in this study, including 27 men and 16 women, with ages ranging from 25 to 78 (median 65) years old. Clinicopathological profiles of the patients and their HCCs are shown in Table 1. Antibody to hepatitis C virus was found in sera of 72% of the patients, and hepatitis B virus surface antigen was positive in 21%.

According to the TNM staging, 60% were stage I to II and 40% were stage III to IV. In noncancerous portions of the resected livers, cirrhosis and chronic hepatitis[18] were found in 68% and 30%, respectively, of the specimens, whereas only 1 (2%) was of normal histology. Fibrocapsular formation surrounding HCC was observed in 84% and capsular invasion by HCC cells in 33%. Portal vein involvement and satellite nodules suggesting intrahepatic metastasis were found in 21% and 37%, respectively.

Detection of Gankyrin with the Monoclonal Anti-gankyrin Antibody. To determine the specificity of the monoclonal anti-gankyrin antibody 3A6C2, we expressed wild-type full-length or truncated gankyrin (Fig. 1A) in 293T cells. The antibody detected all mutants of gankyrin, suggesting that the epitope exists within the third and fifth ankyrin-repeat region (Fig. 1B). The antibody recognized the endogenous gankyrin as well, and no major cross-reacting band was observed.

Because gankyrin mRNA is known to be overexpressed in most HCCs,[9] we analyzed the levels of gankyrin protein in HCCs and surrounding noncancerous liver tissues using the 3A6C2 antibody. The protein level of gankyrin was higher in HCC tissues than in noncancerous tissues

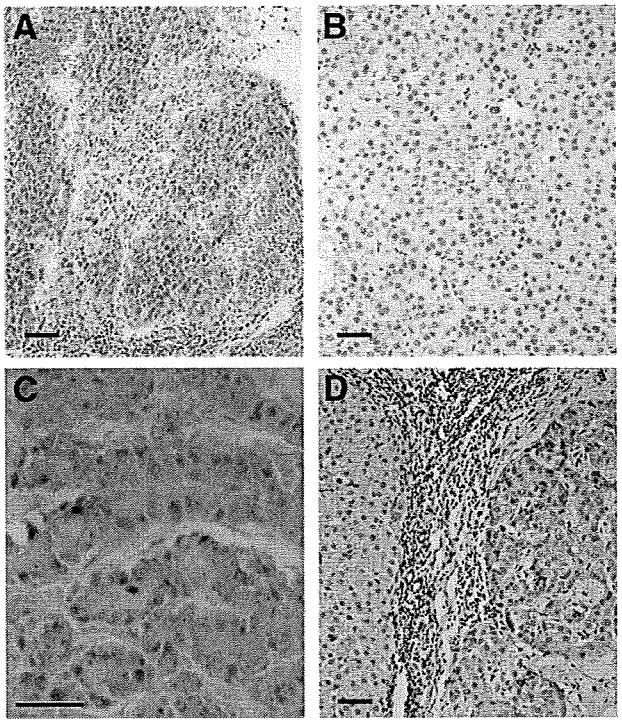

Fig. 2. Immunohistochemical detection of gankyrin in hepatocellular carcinoma (HCC). HCC sections were stained with mouse monoclonal anti-gankyrin antibody, and counterstained with hematoxylin. Positive immunostaining appears brown. (A) Positive staining for gankyrin in the cytoplasm of most HCC cells. (B) Barely detectable gankyrin signal in some HCC cells. (C) Presence of gankyrin in the nucleus of some HCC cells. (D) Stronger staining for gankyrin in HCC cells (right) than the neighboring cirrhotic hepatocytes (left). Bar, 50 μm.

(Fig. 1C). The mobilities of the gankyrin band were not different among samples.

Immunohistochemical Analysis of Gankyrin Expression. We next examined the expression of gankyrin protein in HCC and noncancerous liver tissues by immunohistochemistry. The gankyrin signal was observed mainly in the cytoplasm and occasionally in the nucleus of HCC cells (Fig. 2A-C). Although at lower levels compared with those in HCCs, weak but reproducible gankyrin signals were observed in the cytoplasm of the hepatocytes in the noncancerous tissues (Fig. 2D). Expression of gankyrin was not detected in the bile duct cells, blood endothelial cells, or other nonparenchymal cells in the liver tissues. Of 43 HCCs examined, the cytoplasm was stained positively for gankyrin in 27 (63%), and 9 of them (21%) were also positive for nuclear staining. Of 32 noncancerous liver tissues available, gankyrin was positive in 17 (53%).

As shown in Table 2, we analyzed an association between gankyrin protein expression and clinicopathological findings. No significant association between gankyrin expression in HCC cells and sex, age, tumor size, fibrotic change in noncancerous liver tissues, differentiation of the tumor cells, or hepatitis B or C virus infection was observed. Positive cytoplasmic staining for gankyrin of HCC cells was significantly associated with low TNM stage (stage I or II; $P = 0.004$), no capsular invasion ($P = 0.018$), no portal venous invasion ($P = 0.008$), and no intrahepatic metastasis ($P = 0.012$) of HCC. In noncancerous liver tissues, positive gankyrin staining of hepatocytes was associated with the cytoplasmic gankyrin positivity of HCC cells of the same patient ($P = 0.021$, Table 3), but not with the parameters examined except for the serum alpha-fetoprotein level ($P = 0.015$, Table 2).

Because expression of gankyrin affects the degradation of p53 and MDM2,[16] we examined the expression of p53 and MDM2 as well as gankyrin in HCCs. By immunohistochemistry, nuclear expression of p53 and MDM2 were detected in 30% and 23%, respectively, of 43 HCCs (Fig. 3, Table 3). Positive staining for gankyrin was not associated with the staining for p53 nor MDM2 in HCC cells.

Up-regulation of IGFBP-5 Expression by Gankyrin in HCCs. Preliminary microarray analysis of the cDNA libraries prepared from U-2 OS cells and Huh-7 cells overexpressing gankyrin suggested that IGFBP-5 mRNA was up-regulated by gankyrin (A. Umemura and J. Fujita, unpublished data). Real-time RT-PCR analysis con-

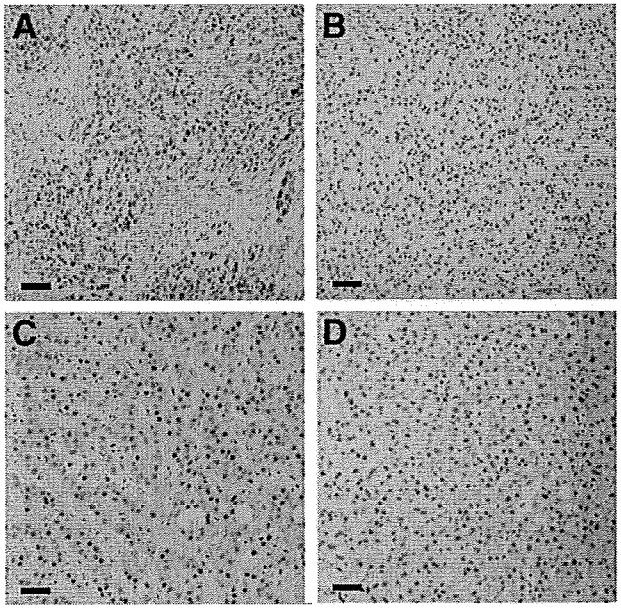

Fig. 3. Immunohistochemical detection of p53 and MDM2 in hepatocellular carcinoma (HCC). HCC sections were stained with antibodies specific to p53 (A and B) or MDM2 (C and D), and counterstained with hematoxylin. Positive immunostaining appears brown. (A) Positive staining for p53 in the nucleus of most HCC cells. (B) Negative p53 in HCC cells. (C) Positive staining for MDM2 in the nucleus of most HCC cells. (D) Negative MDM2 in HCC cells. Bar, 50 μm.

Table 2. Gankyrin Expression and Clinicopathological Characteristics

	Gankyrin Expression in the Cytoplasm of					
	HCC			Noncancerous Liver		
	Negative (n = 16)	Positive (n = 27)	*P* value	Negative (n = 15)	Positive (n = 17)	*P* value
Sex distribution						
Male	12	15	0.328	10	11	1.000
Female	4	12		5	6	
Median age (years)	64	65	0.696	63	62	0.649
Virus marker			NS			NS
HBV(+)/HCV(−)	3	3		2	2	
HBV(−)/HCV(+)	10	18		11	11	
HBV(+)/HCV(+)	1	2		2	0	
HBV(−)/HCV(−)	2	4		0	4	
Median AFP (ng/mL)	63.0	95.0	0.890	25.0	199.0	0.015
Median tumor size (cm)	4.5	4.0	0.098	4.5	4.0	0.372
Liver cirrhosis (+)	9	20	0.316	9	13	0.450
TNM stage						
I and II	5	21	0.004	8	12	0.467
III and IV	11	6		7	5	
Histological differentiation						
Well	5	7	0.737	6	3	0.243
Moderate and poor	11	20		9	14	
Capsular formation (+)	15	21	0.229	12	13	1.000
Capsular invasion (+)	9	5	0.018	4	6	0.712
Portal venous invasion (+)	7	2	0.008	4	3	0.678
Intrahepatic metastasis (+)	10	6	0.012	6	5	0.712
Gankyrin nuclear expression						
Yes	0	9	0.016	2	5	0.403
No	16	18		13	12	

Abbreviations: HCV, anti-hepatitis C virus antibody; HBV, hepatitis B surface antigen; (+), positive or present; (−), negative or absent; AFP, serum alpha-fetoprotein; NS, not significant between any groups or combinations thereof.

firmed that overexpression of gankyrin increased the IGFBP-5 mRNA levels 5.2-fold and 1.7-fold (mean, n = 3 each) in U-2 OS and Huh-7 cells, respectively, and western blot analysis demonstrated that the protein levels were increased as well (Fig. 4A). Conversely, when gankyrin expression was suppressed by siRNA, IGFBP-5 expression was down-regulated (Fig. 4B). In 2 of 3 HCC tissues overexpressing gankyrin, the levels of IGFBP-5 protein were higher compared with those in noncancerous tissues (Fig. 1C). To identify a role that IGFBP-5 might play in HCC cells, we next suppressed IGFBP-5 expression by siRNA. No apoptosis was induced, but viable cell numbers were decreased in Huh-7 as well as U-2 OS cells (Fig. 4C,D, and data not shown), suggesting a growth-promoting effect of IGFBP-5.

The expression of IGFBP-5 was further examined immunohistochemically in 43 HCC and 32 noncancerous liver tissues (Fig. 5, Table 3). In 42% of HCCs, IGFBP-5 was positively stained in the cytoplasm of HCC cells (Fig. 5A). IGFBP-5 was also detected, although at lower levels, in the cytoplasm of hepatocytes in 28% of the noncancerous tissues (Fig. 5B-D), but not in bile duct cells, blood endothelial cells, or other nonparenchymal cells.

Specific cytoplasmic staining for IGFBP-5 in HCC cells was associated with low TNM stage (stage I or II; $P = 0.013$), no portal venous invasion ($P = 0.006$), low serum alpha-fetoprotein value ($P = 0.031$), and small tumor size ($P = 0.009$). No association with capsular invasion or intrahepatic metastasis was observed. There was a significant association between positivities for IGFBP-5 and

Table 3. Gankyrin Expression and Molecular Histological Markers

	Gankyrin Expression in HCC		
	Negative	Positive	*P* value
Gankyrin expression in non-HCC			
Negative (n = 15)	8	7	0.021
Positive (n = 17)	2	15	
p53 expression in HCC			
Negative (n = 30)	11	19	1.000
Positive (n = 13)	5	8	
MDM2 expression in HCC			
Negative (n = 33)	14	19	0.276
Positive (n = 10)	2	8	
IGFBP-5 expression in HCC			
Negative (n = 25)	13	12	0.026
Positive (n = 18)	3	15	
IGFBP-5 expression in non-HCC			
Negative (n = 23)	14	9	0.011
Positive (n = 9)	1	8	

Abbreviations: HCC, hepatocellular carcinoma; non-HCC, noncancerous portion of the resected liver; IGFBP-5, insulin-like growth factor-binding protein 5.